ABSTRACT

Title of Dissertation: UNIFYING SEARCHES FOR NEW PHYSICS WITH PRECISION MEASUREMENTS OF THE W BOSON MASS

Deepak Sathyan
Doctor of Philosophy, 2024

Dissertation Directed by: Professor Kaustubh Agashe
Department of Physics

The Standard Model (SM) of particle physics has been extremely successful in describing the interactions of electromagnetic, weak nuclear, and strong nuclear forces. Yet, there are both unexplained phenomena and experimentally observed tensions with the SM, motivating searches for new physics (NP).

Collider experiments typically perform two kinds of analyses: direct searches for new physics and precision measurements of SM observables. For example, experimental collaborations use collider data to search for NP particles like the heavy superpartners of the SM particles, whose observation would be clear evidence of supersymmetry (SUSY). These direct searches often consider kinematic regions where the SM background is small. This strategy is unable to probe regions of the NP parameter space where the SM background is dominant.

The same collaborations also measure the masses of SM particles, which not only serve as consistency tests of the SM, but can also probe effects of NP. In 2022, the Collider Detec-

tor at Fermilab (CDF) collaboration published the most precise measurement of the W boson mass: m_W = 80433.5 $\pm$ 9.4 MeV. This measurement is in 7σ significance tension with the SM prediction via the electroweak (EW) fit, $m_W^{\text{pred.}}$ = 80354 $\pm$ 7 MeV. Many extensions to the SM can affect the prediction of m_W with indirect effects of heavy NP. However, in 2023, the ATLAS re-measurement of the W boson mass, m_W = 80360 $\pm$ 16 MeV, was found to be consistent with the SM prediction. Both collaborations found a high-precision agreement between the measured kinematic distributions and the SM prediction of the kinematic distributions for their corresponding extracted m_W.

We propose using the precision measurements of m_W to directly probe NP contributing to the same final state used to measure m_W: a single charged lepton ℓ and missing transverse energy $\not{E}_T$. This strategy is independent of modifying the EW fit, which tests indirect effects of NP on the predicted value of m_W. Any NP producing $\ell + \not{E}_T$ which modifies the kinematic distributions used to extract m_W can be probed with this method. With this strategy, since these distributions are used to search for NP while measuring m_W, a simultaneous fit of NP and SM parameters is required, thus unifying searches and measurements. This simultaneous fitting can induce a bias in the measured m_W, but only to a limited extent for our considered models.

We consider three categories of NP which can be probed: (i) modified decay of W bosons; (ii) modified production of W bosons; and (iii) $\ell + \not{E}_T$ scenarios without an on-shell W boson. We also show that models whose signals extend beyond the kinematic region used to measure m_W can be probed in an intermediate kinematic region. Our results highlight that new physics can still be discovered at the LHC, including light new physics, via SM precision measurements. Additionally, anticipated improvements in precision SM measurements at the High Luminosity LHC further enables new searches for physics Beyond the Standard Model (BSM).

Unifying Searches for New Physics with Precision Measurements of the W Boson Mass

by

Deepak Sathyan

Dissertation submitted to the Faculty of the Graduate School of the
University of Maryland, College Park in partial fulfillment
of the requirements for the degree of
Doctor of Philosophy
2024

Advisory Committee:
Professor Kaustubh Agashe, Chair/Advisor
Professor Tom Cohen
Professor Sarah Eno
Professor Raman Sundrum
Professor Richard Wentworth

Dedication

To my parents, Sathyan and Sreedevi, and my brother, Vineet, for their support and encouragement...

Acknowledgments

Throughout my time as a PhD student, I've been truly fortunate to spend time with caring friends, helpful and supportive colleagues, and compassionate and wise mentors.

I'd first like to thank my advisor, Professor Kasutubh Agashe, for his patience, mentorship, encouragement, and opportunity to work with him on research projects over the last 5 years. I've learned so much about particle physics, phenomenology, collider physics, and more through my discussions with him. I'll always be extremely thankful for his willingness to discuss physics but also his flexibility, especially during the pandemic.

Next, I'd like to thank all my collaborators during my time as a PhD student. I've enjoyed my many meetings with Doojin Kim, Majid Ekhterachian, Roberto Franceschini, Sagar Airen, Lorenzo Ricci, Joe Incandela, Ashutosh Kotwal, Bhupal Dev, Kuver Sinha, Yongchao Zhang, Amit Bhoonah, Da Liu, and Tong Ou. My interactions and discussions with my collaborators kindles my interest in exploring particle physics and thinking about new, interesting ideas.

Many of the courses I took in graduate school were taught by the other faculy in our group: I owe much of my education in high energy physics to Professor Raman Sundrum, Professor Anson Hook, and Professor Zackaria Chacko.

Much of my time outside of physics was spent with my partner Bekah Wong, my closest friends Sanket Doshi and Emily Jiang, and my roommates I had for many years: Saurabh Kadam, Mike Winer, and William Grunow. I truly appreciate the time spent them in so many ways like cooking food, going out to restaurants, playing games, chatting, and watching TV and movies. The time I spend with those closest to me is that which I cherish most.

I also truly appreciate the conversations and interactions I had with other students and post-docs in the department, notably Saurav Das, Arushi Bodas, Dawid Brzeminski, Ed Broadberry, Ina Flood, Chung-Chun Hseih, Abhishek Banerjee, Alex Fernez, and Andy Sheng.

I'd also like to thank the committee members, including Professor Tom Cohen, Professor Richard Wentworth, and Professor Sarah Eno, for their time and discussions.

Lastly, I want to give my appreciation to my parents and my brother for their support not only throughout my academic journey, but my entire life. They have been there for me always, and I would not have made it this far without their encouragement, support, and compassion.

There are many others who have had an impact on me during my time as a PhD student, but it is impossible to list them all. My sincerest apologies to anyone I inadvertently did not name.

Table of Contents

List of Tables

List of Figures

List of Abbreviations

NP	New Physics
SM	Standard Model
SUSY	Supersymmetry
MSSM	Minimal Supersymmetric Standard Model
BSM	Beyond the Standard Model
EW	electroweak
EWSB	electroweak symmetry breaking
VEV	vacuum expectation value
LHC	Large Hadron Collider
CDF	Collider Detector at Fermilab
SPS	Super Proton Synchrotron
DM	Dark Matter
QED	Quantum Electrodynamics
QFT	Quantum Field Theory
EM	Electromagnetic
SSB	Spontaneous Symmetry Breaking
LEP	Large Electron-Positron
ISR	Initial State Radiation
RPV	R-Parity-Violating
LSP	Lightest Supersymmetric Particle
MC	Monte Carlo
DY	Drell-Yan
HL	High Luminosity

Chapter 1: Introduction

The field of particle physics is at an interesting crossroads. While the Standard Model (SM) of particle physics has been extremely successful in describing three of the four fundamental interactions, specifically the electromagnetic, weak nuclear, and strong nuclear forces, there are limitations of the SM and hints of new physics (NP). The motivations for extensions to the SM are discussed further.

Ultimately, the SM is an effective field theory description of nature, not the complete picture. In particular, the SM currently does not contain a renormalizable theory of gravity. Furthermore, the scale at which quantum gravitational interactions become important, the Planck mass $m_{Pl} \sim 10^{19}$ GeV, is at a vastly different scale than the electroweak scale $m_{EW} \sim \mathcal{O}(100)$ GeV, creating a hierarchy problem. There also exists the flavor hierarchy between masses of different flavors of quarks. While these hierarchies are not necessarily inconsistencies of the model, there are theories of physics beyond the Standard Model (BSM) such as supersymmetry (SUSY) or Randall-Sundrum models which attempt to resolve these hierarchy problems, but no clear signs of NP have been observed at experiments like the Large Hadron Collider (LHC).

Additionally, there are phenomena unexplained by the SM: dark matter, dark energy, neutrino masses, and matter-antimatter asymmetry are a few notable examples. While gravitational effects of dark matter (DM) have been observed, there are many models which predict nongravitational interactions of DM with the SM. The ability to probe such models is an aspect of the work described in this thesis.

Direct searches for NP particles have found nothing definitive thus far. However, there are experimental observations which could be in tension with SM predictions. For example, the 2022 Run 2 measurement of the W boson mass m_W by the Collider Detector at Fermilab (CDF) experimental collaboration is 7σ away from the SM prediction of m_W [4], the measurement of the anomalous precession frequency of the muon $(g-2)_\mu$ at Fermilab is also in tension with the SM prediction [15–18].[1]

Many physicists considered introducing some heavy new physics which modifies the electroweak (EW) fit prediction of the W boson mass to more closely match CDF's measured value of m_W, seen in [19, 20] for example. Within the SM electroweak theory, m_W and other observables can be predicted in terms of the precisely measured quantities: G_F, m_Z, and α_{QED}, taken as input parameters. The EW fit then compares these predictions to measurements of these observables [21, 22]. However, the story is further complicated by the ATLAS re-measurement of their Run 1 data, published a year later in 2023, which was found to be consistent with the EW fit prediction [3]. A summary of the measurements of m_W and the EW fit prediction is shown in Fig. 2.7.

My collaborators and I instead propose harnessing the precision of these W boson mass measurements to probe direct effects of NP which could contaminate the distributions of observables used to extract m_W. Since the precision measurements of m_W consider the leptonic decay of the W boson ($\ell + \not{E}_T$), where $\not{E}_T$ is missing energy in the transverse plane, shown in Fig. 2.5b,

[1]The theoretical predictions of $(g-2)_\mu$ are a bit murky at this time. Lattice calculations disagree with the data-driven predictions of the $(g-2)_\mu$ theory initiative. The measurement is in $> 5\sigma$ tension with the theory initiative prediction, but less so with the lattice prediction.

the events are not fully reconstructible since the neutrinos appear as missing energy to the detectors. Thus, such a final state is a good hideout for invisible NP, such as particles coupled to dark sectors. However, since experimental collaborations have found that the measured kinematic distributions agree very well with SM predictions, any NP which produces the same final state yet modifies the kinematics could be excluded.

Probing NP with this procedure requires a simultaneous fit of NP and SM parameters, often floating the NP particle mass and coupling simultaneously with m_W extracted from a fit to the kinematic distributions. This simultaneous fit can also induce a bias in the extracted m_W to compensate for allowed nonzero NP in the sample.

Ultimately, we find that precision measurements of m_W can place competitive or even exceed bounds on NP models which produce $\ell + \not{E}_T$ while either (A) modifying W boson decay, (B) modifying W boson production, or (C) not requiring an on-shell W boson. The concrete examples of NP we consider are (A) the leptophilic $L_\mu - L_\tau$ Z' boson, neutrinophilic scalar ϕ, and heavy neutrino ν_4, (B) hadrophilic Z' boson, and (C) slepton-sneutrino production in the Minimal Supersymmetric Standard Model (MSSM).

We consider two kinematic regions to search for new physics in $\ell + \not{E}_T$, which are shown in Fig. 1.2. Before going into the details of each region we propose to search for NP, it is important to understand the current landscape of searches and measurements. Generally, searches are often conducted in kinematic regions where the background from the SM is small. This is intuitive since an excess of events found in these regions are clear signs for some heavy new physics. However, this search strategy can only probe effects of heavy new physics. This is shown schematically in Fig. 1.1. To probe light new physics whose signals are too faint to probe in this high energy regime, we must consider searching in SM-dominant regions. The modeling

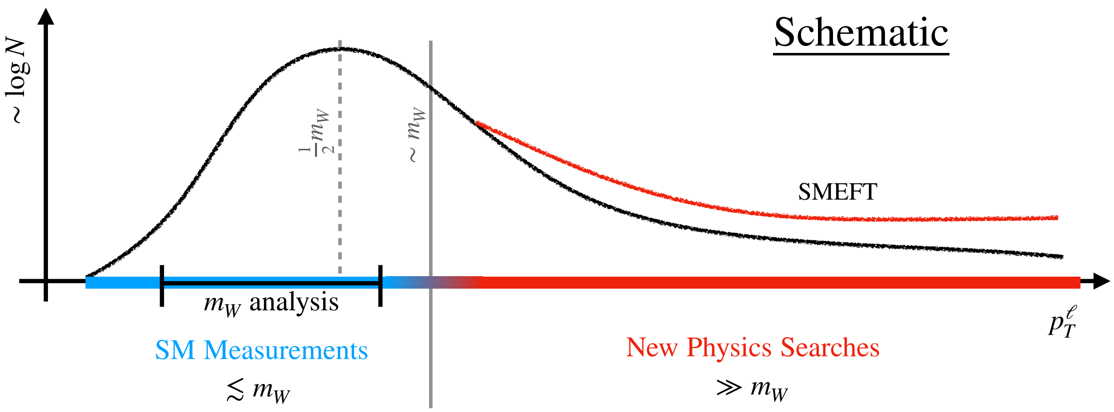

Figure 1.1: Sketch of the searches and measurements regions in the usual approach. In black, we show a schematic distribution of the transverse momentum of the lepton from the SM decay of the W boson, with the Jacobian peak at $^1/_2 m_W$. The blue region shows where the measurements of SM parameters take place, like m_W and Γ_W. The red region shows where searches for heavy new physics like W' and SM Effective Field Theory (SMEFT) operators occur. The red line shows roughly where the distribution would change with the inclusion of heavy BSM physics.

of SM backgrounds must be precise enough to be sensitive to changes in the shapes of measured distributions by NP. This is exactly what the recent W mass measurements can do for us.

The first region where we propose searching for light NP is near the Jacobian peak at $m_W/2$ in transverse momentum of the lepton, which we call the sub-electroweak (sub-EW) region. This kinematic region is highly sensitive to the W boson mass, since this is where events used to extract m_W lie. Any new physics which modifies the kinematic distributions below or near the Jacobian peak can be probed here, but the sub-EW strategy requires the simultaneous extraction of NP parameters with m_W. Category (A) of NP models which modifies the decay of the W boson will often soften the charged lepton's momentum distribution, and thus the sub-EW strategy is the clear option. However, even NP which affects the kinematics at higher p_T, such as those in categories (B) and (C), can also be probed in the sub-EW region. Since the sub-EW region overlaps strongly with the W boson mass measurement, we aim to analyze the NP using the m_W measurement as guidance for cuts on events, etc. We will propose small extensions to the

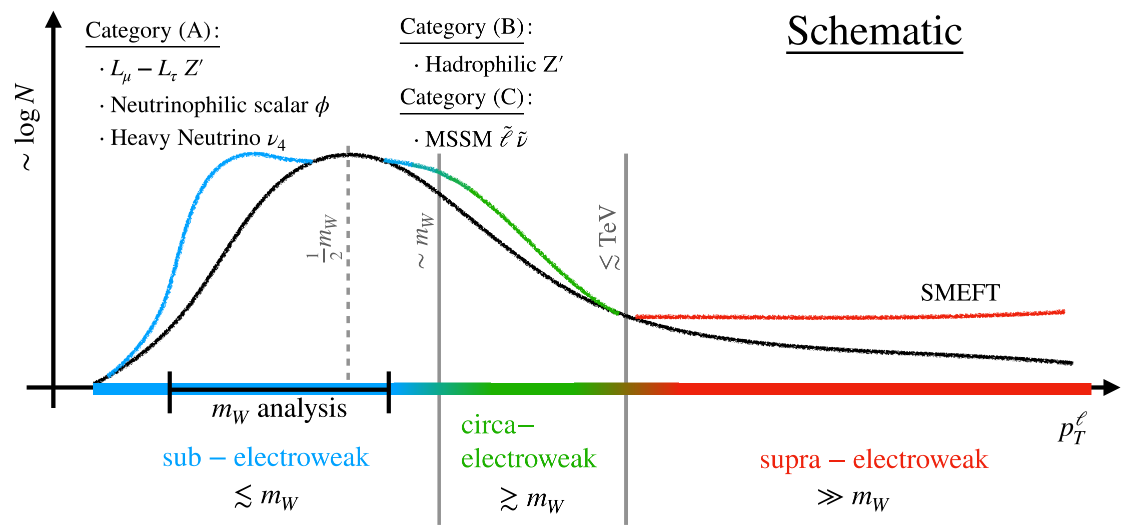

Figure 1.2: Sketch of the various analysis regions considered in this paper. In black, we show a schematic distribution of the transverse momentum of the lepton from the SM decay of the W boson. The colored lines show roughly where the distribution would change with the inclusion of various BSM physics. The **sub-electroweak** region contains the Jacobian peak [5] at $\frac{1}{2}m_W$ of the SM W boson distributions, and is therefore used to measure m_W: the systematic uncertainties here can reach the per-mill level [2–4]. The **supra-electroweak** region contains the high-p_T tails of the distributions and is often used for heavy BSM physics searches, like for W' [6], where the systematic uncertainties are usually $\sim 10\%$. In between these regions, just above the Jacobian peak, we identify a **circa-electroweak** region, which holds opportunity for BSM discovery for per-cent level systematics.

kinematic region to increase the sensitivity to NP.

However, it turns out we can increase the sensitivity to NP in categories (B) and (C) which modify the kinematics well above the Jacobian peak. In the transverse momentum space, this corresponds to the kinematic region $\geq m_W$, which we call the "circa-electroweak" (circa-EW) region. This region is different from the standard search region in Fig. 1.1 because it does not extend to TeV-scale energies. Instead, we propose a more targeted search for NP whose kinematics can significantly modify the measured distributions in this intermediate region. There are a number of additional factors to consider in this region which are different from the sub-EW analysis. In particular, we must now consider which set of cuts to impose to isolate events in this region, additional backgrounds, uncertainties on the luminosity, and larger per-bin systematics for the fit.

Lastly, there is a third region beyond the circa-EW region, denoted the "supra-electroweak" (supra-EW) region. This is analogous to the usual search strategy in Fig. 1.1, where effects of heavy NP are searched for in a relatively SM-background-free environment [23]. Since we are probing light new physics, the signals from the models we consider will not produce enough signal events in the supra-EW region to probe. Therefore, we only search for NP in the sub- and circa-EW regions.

The rest of this thesis is structured as follows: the theoretical and experimental history of the W boson and its mass are presented in Chapter 2, followed by a description of the new purpose of precision measurements of m_W. Then, in Chapter 3, the categories of new physics models are stated, with motivations and descriptions of each model. Then the analysis for probing NP in the sub-electroweak and circa-electroweak regions are presented in detail in Chapter 4 and Chapter 5, respectively, followed by concluding remarks in Chapter 6.

Chapter 2: Prediction and Measurements of the W Boson Mass

In this chapter, a review of the Standard Model of particle physics will be presented, leading up to the prediction of the W boson mass after electroweak symmetry breaking (EWSB). Then, the focus shifts to experimental observations of the W boson and in particular, the most recent measurements of the W boson mass by the CDF and ATLAS collaborations. Finally, with the necessary background, I will present our idea to probe light new physics using precision measurements of m_W.

2.1 A Review of the Standard Model

The SM of particle physics is a quantum field theory which describes the fundamental particles and their interactions, not including gravitational interactions. The particles in the SM are categorized by their spin: matter fields are spin-$1/2$ particles called fermions. The fermions are further categorized into quarks and leptons, each of which contains six particles grouped into three generations. The first generations of leptons and quarks make up the lightest matter fields, which are stable. The second and third generations contain heavier, unstable quarks and leptons, which can decay to the lighter generations. The force carriers are spin-1 particles which allow quarks and leptons to interact. Gluons are the massless force carrier of the strong nuclear force, confining quarks into composite states like hadrons (protons, neutrons) and mesons (pions, Kaons, etc.). Photons are the massless force carrier of the electromagnetic force, allowing interactions between electrically charged particles. The W and Z bosons are the massive force carriers of the weak nuclear force, which can produce charged ($W^{\pm}$) or neutral (Z) currents between quarks and leptons. Lastly, a spin-0 particle called the Higgs boson corresponds to the Higgs field, which gives quarks, leptons, and the weak force carriers their mass. The particle content of the SM is visually depicted in Fig. 2.1.

The SM is a non-Abelian gauge theory with interactions obeying the symmetry group $SU(3)_C \times SU(2)_L \times U(1)_Y$. Each gauge group corresponds to one of the forces described by the theory: $SU(3)_C$ is the gauge group of quantum chromodynamics, and $SU(2)_L \times U(1)_Y$ is the gauge group for the electroweak interactions, with L denoting left-handed particles in weak isospin doublets and Y denoting weak hypercharge. These interactions connect quarks to leptons, but the symmetry group on its own predicts massless gauge bosons, in disagreement with observations of weak interactions. Spontaneous symmetry breaking through the Higgs mechanism [24] breaks $SU(2)_L \times U(1)_Y \to U(1)_{EM}$, leaving only the photon to be massless among the electroweak gauge bosons.

The SM accurately predicted the existence of particles which have been experimentally observed such as the W and Z bosons. One of the achievements of the standard model is the unification of the weak nuclear force with the electromagnetic force into the theory of electroweak interactions under the symmetry group $SU(2)_L \times U(1)_Y$. This symmetry is spontaneously broken by the Higgs mechanism, reducing the symmetry to $U(1)_{\text{EM}}$ with a massless photon, while making the W and Z bosons massive. The discovery of the Higgs boson at the Large Hadron Collider in 2012 [25, 26] experimentally validated both the Higgs mechanism of spontaneous symmetry breaking and the Standard Model itself. In this chapter, I will briefly summarize the

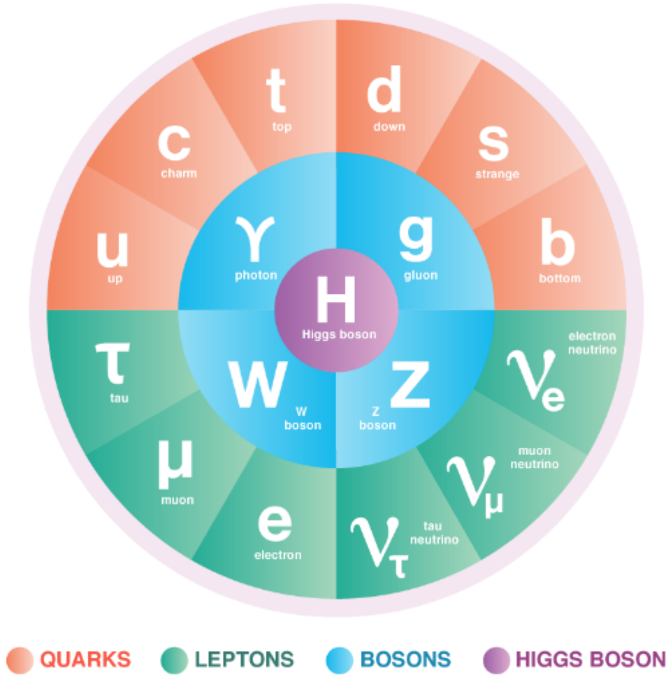

Figure 2.1: A visual representation of the Standard Model of particle physics [7]. The fermion matter fields are on the outside, with quarks on the top half and leptons on the bottom half. The gauge bosons which mediate the forces and interactions among leptons and quarks are inside, with the Higgs boson at the center.

relevant aspects of the SM leading up to the prediction of the W boson and its mass. Then I will discuss the experimental observations of the W boson and the recent measurements of its mass m_W. Finally, I will describe the new purpose of the precision measurements of m_W to probe light new physics (NP), which is the main focus of this thesis.

2.1.1 QED Lagrangian

We begin with a brief description of quantum electrodynamics (QED). It is historically the first defined relativistic quantum field theory (QFT) The model of electrodynamics should describe interactions of electrically charged particles with the corresponding force carrier: the photon. QED is an Abelian gauge theory with a symmetry group $U(1)$, with local gauge transformations given by

$$\psi(x) \to \psi'(x) = \psi(x)e^{i\alpha(x)}. \tag{2.1}$$

In the above equation, ψ is a Dirac fermion field of mass m, which satisfies the Dirac equation:

$$(i\gamma^{\mu}\partial_{\mu} - m)\psi(x) = 0, \tag{2.2}$$

where γ^{μ} are the well-known gamma (or Dirac) matrices. The Lagrangian of quantum electrodynamics is given by

$$\mathcal{L}_{\text{QED}} = \bar{\psi}(i\gamma^{\mu}D_{\mu} - m)\psi - \frac{1}{4}F_{\mu\nu}F^{\mu\nu}, \tag{2.3}$$

where $D_{\mu} = \partial_{\mu} + ieA_{\mu}$ is the gauge covariant derivative, e is the electric charge, A_{μ} is the electromagnetic (EM) or photon field, and $F_{\mu\nu} = \partial_{\mu}A_{\nu} - \partial_{\nu}A_{\mu}$ is the EM field strength tensor. This Lagrangian combines the free Dirac equation for the electron, the Maxwell equations for the EM field, and the interaction between them. In particular, the interaction term between the fermion and the EM field is contained in the gauge covariant derivative.

One of the most remarkable aspects of QED is its renormalizability, a way of handling infinities that arise in QFT calculations. By redefining the parameters of the theory, such as the charge and mass of the electron, renormalization gives the ability to make finite and accurate predictions. QED has been vigorously tested experimentally, for example, with measurements of the electron's anomalous magnetic moment. However, it alone does not describe other interactions observed in nature, such as neutron decay. Such processes are interactions of the weak nuclear force.

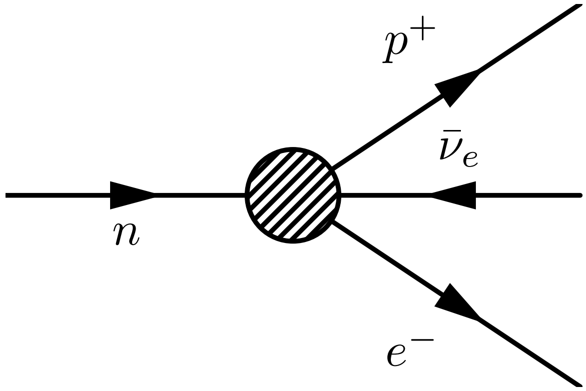

(a) β Decay in Fermi theory

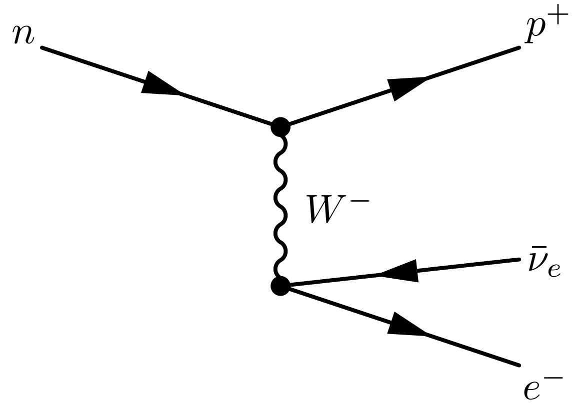

(b) β Decay in EW theory

Figure 2.2: Feynman diagrams of β decay, converting a neutron into a proton, electron, and electron-antineutrino, (a) as a contact interaction in Fermi theory and (b) through a W^- boson in EW theory. The observations of β decay was one of the first signs of the weak nuclear force.

2.1.2 Electroweak Lagrangian

In the 1930s, Enrico Fermi constructed an effective field theory description of the weak nuclear force to describe beta decay. Fermi proposed a four-fermion effective interaction to model β decay shown in Fig. 2.2a, coupling the neutron to a proton, electron, and anti-neutrino through a contact interaction: $n^0 \to p^+ e^- \bar{\nu}_e$. However, the Fermi effective interaction coupling G_F is dimensionful, $[G_F] = [m^{-2}]$, making the theory non-renormalizable.

Then in the 1960s, Sheldon Glashow, Abdus Salam, and Steven Weinberg developed the gauge theory of electroweak interactions [27–29]. This gauge theory predicts that processes like β decay are mediated by a massive gauge boson as shown in Fig. 2.2b. In the low energy limit, this interaction reduces to the contact interaction in Fermi theory. Furthermore, this gauge theory is renormalizable like QED if the masses of the gauge bosons arises from the Higgs mechanism of spontaneous symmetry breaking (SSB), as described in the following section.

The gauge group describing the weak nuclear force also includes the gauge group of electrodynamics, hence a Lagrangian which unifies the electromagnetic and weak nuclear forces into the electroweak (EW) theory. The EW Lagrangian is given by

$$\mathcal{L}_{\text{EW}} = \mathcal{L}_g + \mathcal{L}_f + \mathcal{L}_h + \mathcal{L}_y, \tag{2.4}$$

where $\mathcal{L}_g$ contains the gauge boson interactions, $\mathcal{L}_f$ contains the fermion kinetic terms, $\mathcal{L}_h$ describes the Higgs field and its interactions with the gauge bosons, and $\mathcal{L}_y$ describes the Yukawa interactions between the Higgs and the fermions.

Expanding each of these Lagrangian terms and describing them in more detail:

$$\mathcal{L}_g = -\frac{1}{4}W^a_{\mu\nu}W^{a\mu\nu} - \frac{1}{4}B_{\mu\nu}B^{\mu\nu} \tag{2.5}$$

describes the interactions between the three W bosons and the B boson. The W and B here are the field strengths for weak isospin and weak hypercharge gauge fields, respectively. A linear combination of W^1 and W^2 will result in the $W^{\pm}$ bosons, and a combination of W^3 and B will give the Z boson and photon γ.

Next the fermion Lagrangian is given by

$$\mathcal{L}_f = \bar{\psi}_L i\gamma^\mu D_\mu \psi_L + \bar{\psi}_R i\gamma^\mu D_\mu \psi_R, \tag{2.6}$$

where ψ_L and ψ_R are the left- and right-handed fermion fields in the SM. In particular, psi_L contains Q and L, representing the left-handed doublets of quarks and leptons. The right-handed singlets u, d, and e for up, down, and charged leptons are contained in ψ_R. The gauge covariant derivative D is modified in electroweak theory to

$$D_\mu = \partial_\mu - i\frac{g'}{2}YB_\mu - i\frac{g}{2}T_j W^j_\mu, \tag{2.7}$$

where Y is the weak hypercharge and T_j are the components of weak isospin.

The Higgs part of the Lagrangian is given by

$$\mathcal{L}_h = |D_\mu h|^2 - \lambda\left(|h|^2 - \frac{v^2}{2}\right)^2, \tag{2.8}$$

where v is the vacuum expectation value (VEV) of the Higgs field. The VEV becomes nonzero after spontaneous symmetry breaking (SSB), which will provide some of the gauge bosons with a mass term.

Lastly, there is the Yukawa interaction between the Higgs boson and fermions, given by

$$\mathcal{L}_y = -\left(y_e \bar{L} h e_R + y_d \bar{Q}\Phi d_R + y_u \bar{Q}\tilde{\Phi} u_R + \text{h.c.}\right). \tag{2.9}$$

These interactions are what give leptons and quarks their masses once the Higgs VEV becomes nonzero after SSB. For a more thorough description of electroweak theory, the Higgs mechanism, etc., the book [30] covers it.

2.1.3 Electroweak Symmetry Breaking

At high energies well above ~ 100 GeV, the electromagnetic and weak nuclear forces are unified in an electroweak force as described earlier. However, below that energy scale, observa-

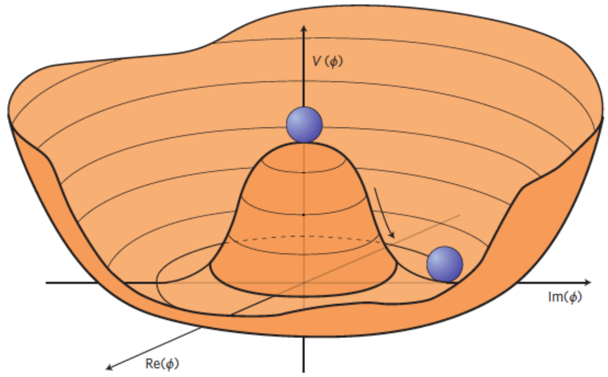

Figure 2.3: A visual depiction of the Higgs potential in which the minimum is no longer at $|\phi|^2 = 0$. The figure is taken from [8].

tions show that these forces behave separately. In other words, the symmetry group that describes the unified electroweak interactions is spontaneously broken. This happens when the Higgs field acquires a nonzero VEV because the Higgs potential has a shape that has a minimum at a nonzero value, as shown in Fig. 2.3.

The Lagrangian after electroweak symmetry breaking (EWSB) is much more complex than prior to the breaking. The relevant aspect of EWSB for the prediction of the W boson mass is that the gauge bosons, which are contained in the covariant derivative coupled to the Higgs field in $\mathcal{L}_h$, acquire masses after expanding the term [1]:

$$
\begin{aligned}
|D_\mu h|^2 &= \frac{1}{8}\left|\begin{pmatrix} gW_\mu^3 + g'B_\mu & \sqrt{2}gW_\mu^- \\ \sqrt{2}gW_\mu^+ & -gW_\mu^3 + g'B_\mu \end{pmatrix}\begin{pmatrix} 0 \\ v \end{pmatrix}\right|^2 \\
&= \left(\frac{1}{2}gv\right)^2 W_\mu^+ W_\mu^- + \frac{1}{8}v^2 (W_\mu^3 \;\; B_\mu)\begin{pmatrix} g^2 & -gg' \\ -gg' & g'^2 \end{pmatrix}\begin{pmatrix} W_\mu^3 \\ B_\mu \end{pmatrix}. \qquad (2.10)
\end{aligned}
$$

From the first term in the expansion, there is now a mass term for $W_\mu^\pm$, given by $m_W = gv/2$. The masses of A_μ and Z_μ can also be obtained by obtaining the coefficients of the eigenstates of the neutral term [1]:

$$\begin{aligned} A_\mu &= \frac{gB_\mu + g'W_\mu^3}{\sqrt{g^2+g'^2}} \ : \ m_A = 0 \\ Z_\mu &= \frac{gW_\mu^3 - g'B_\mu}{\sqrt{g^2+g'^2}} \ : \ m_Z = \frac{v}{2}\sqrt{g^2+g'^2} \end{aligned} \tag{2.11}$$

The relationship between the Z boson mass and W boson mass can be parameterized by the weak mixing angle $\cos\theta_W = \frac{g}{\sqrt{g^2+g'^2}}$, also called the Weinberg angle [27]:

$$\frac{m_W}{m_Z} = \cos\theta_W. \tag{2.12}$$

2.1.4 The prediction of the W Boson Mass

The combination of electroweak theory and Higgs mechanism to generate electroweak symmetry breaking provides a prediction of the masses of the heavy weak force carriers in terms of the coupling constants of the theory and the Higgs VEV: $m_Z = \frac{v}{2}\sqrt{g^2+g'^2}$ and $m_W = gv/2$. Furthermore, this prediction of m_W can be reparameterized in terms of other well-measured constants in the SM: G_F, m_Z, and α_{QED}. With the predictions in hand, experimentalists sought out to observe the existence of these heavy gauge bosons as verification of electroweak interactions. The W and Z bosons were discovered at CERN using the Super Proton Synchrotron (SPS), which collided protons and anti-protons. The UA1 and UA2 collaborations [31, 32] both observed events consistent with W boson decay.

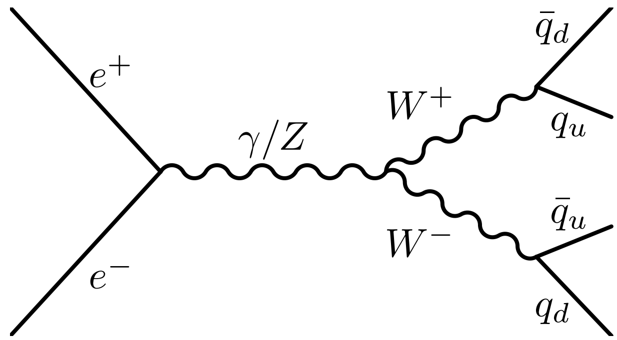

Figure 2.4: One possible Feynman diagram of pair production of W bosons from electron-positron collisions, with hadronic decays used to fully reconstruct the W bosons, as was done at LEP [9]. There is another process which produces a pair of W bosons, through a t-channel exchange of an electron-neutrino.

2.2 A Brief History of W Boson Mass Measurements

After the discovery of the W boson, measurements of the W boson mass were made at the Large Electron-Positron (LEP) collider at CERN [9] and at the Tevatron at Fermilab. Initially, LEP used the hadronic decay of W bosons to fully reconstruct the pair produced W bosons, and found m_W = 80412 $\pm$ 42 MeV, already achieving a 0.5% uncertainty. Fig. 2.4 shows the diagram for hadronic decay of pair produced W bosons at an electron-positron collider.

The m_W experimental value is extracted from the simultaneous fit of different measured kinematic distributions (see below) in leptonic decays of singly-produced W bosons to the SM predictions. Both ATLAS and CDF find perfect agreement with their best-fit SM distributions.

In the following sections, I will describe in more detail the most recent measurements of the W boson mass, and then I will explain how the precision of such measurements allows us to probe new physics which could directly affect the sample of events used to measure m_W.

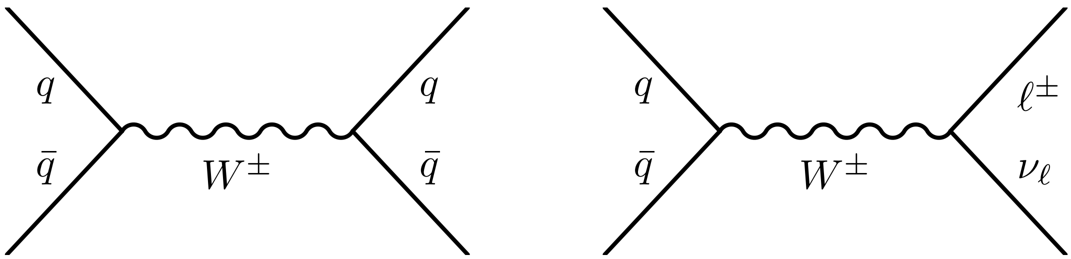

(a) Hadronic Decay (b) Leptonic Decay

Figure 2.5: The two possible SM decay channels for the W boson, produced at hadron colliders. The production of the W boson requires one up-type quark and one down-type quark, resulting in either a positive or negatively charged W boson. When the W decays hadronically, the quarks will form jets, whose energies can be measured at detectors. However, the measurement of jet energies contains large uncertainties. Instead, experiments use the leptonic decay of the W to measure its mass, but this channel is not fully reconstructible since the neutrino is invisible to the detectors. Kinematic distributions like the transverse momentum of the charged lepton p_T^ℓ and the transverse mass m_T are measured precisely. Then, a fit of the SM template of the distribution of the observable $\mathcal{O}$ to the measured distribution of $\mathcal{O}$ is performed. The SM template varies with the input parameter m_W, and m_W is obtained from the best fit.

2.2.1 The CDF Measurement of the W Boson Mass

The Tevatron at Fermilab collides protons and anti-protons at a center-of-mass energy $\sqrt{s} = 1.96$ TeV, which can singly produce $W^\pm$ bosons. The CDF experiment analyzed a sample of $\sim$ 4 million W boson candidate events from a dataset of $\mathcal{L} = 8.8$ fb^{-1} integrated luminosity [4].

CDF considers only the leptonic decay channel to electrons or muons and their anti-matter counterparts, with the associated neutrinos, as shown in Fig. 2.5b. In the case of W^-, the final state would be $e\,\bar{\nu}_e$ or $\mu\,\bar{\nu}_\mu$. The leptonic channel provides cleaner measurements since hadronic final states (Fig. 2.5a) suffer from jet energy scale uncertainties. However, the leptonic decay is not fully visible and therefore not fully reconstructible. Instead, the W boson mass is extracted from fits to kinematic observables, with decays to electrons and muons considered separately.

Before fitting templates to the data, the experiment must impose selection cuts to prop-

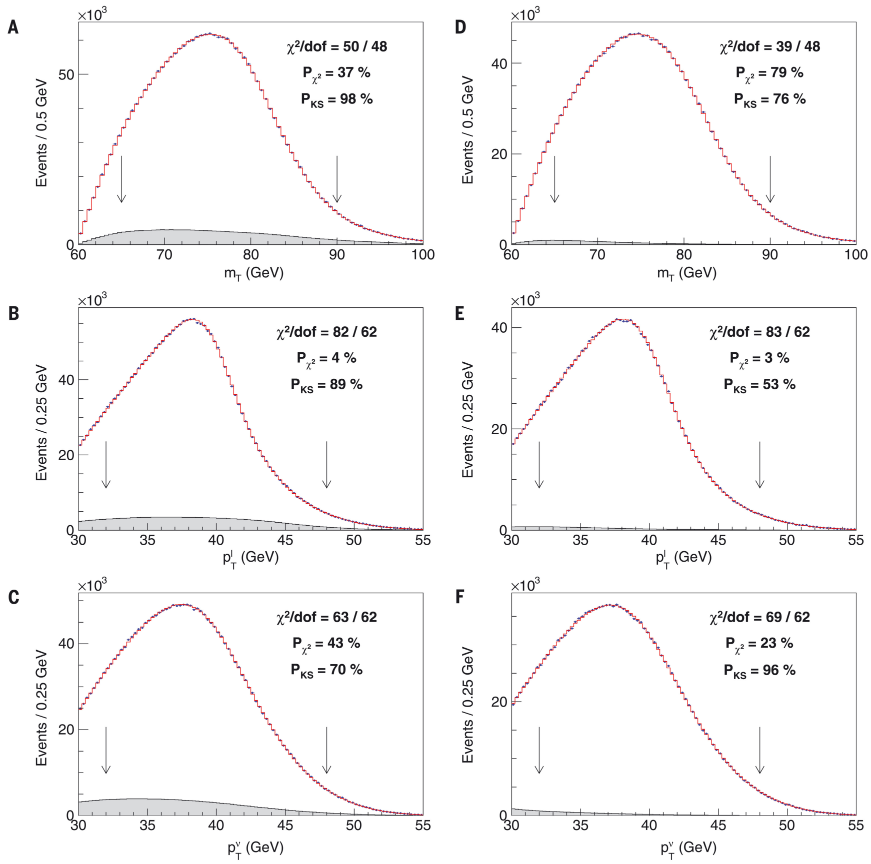

Figure 2.6: Fits of templates of the kinematic observables to the measurements by the CDF collaboration. The blue points are the measured data, and the red line is the template fit to the data, with m_W as a parameter extracted from the fit. The shaded gray regions in each plot indicate the expected number of background events, and the arrows indicate the fitting range.

erly identify events corresponding to leptonic W boson decay. These cuts are summarized in Table 4.1. Candidate events are only selected if there is one electron or muon with a minimum transverse momentum $p_T^\ell > 18$ GeV. Then analysis cuts are imposed, requiring the candidate muon to have at least 30 GeV in p_T, measured in the central region with pseudorapidity $|\eta| < 1$. Any events containing two leptons of the same flavor are rejected, as those events could be background from leptonic Z decays [4]. To further isolate background and purify the event sample to extract m_W, there are additional requirements on the lepton transverse momentum $30 < p_T^\ell < 55$ GeV, missing transverse momentum $30 < p_T^\nu < 55$ GeV, hadronic recoil $|\vec{u}| < 15$ GeV, and transverse mass $60 < m_T < 100$ GeV. Events corresponding to leptonic Z boson decays ($Z \to e^+e^-$, $Z \to \mu^+\mu^-$) are also collected for calibration purposes.

The three kinematic observables used are the transverse momentum of the charged lepton p_T^ℓ, the missing transverse momentum corresponding to the neutrino p_T^ν, and the transverse mass m_T. Templates are constructed to model the distributions expected to be seen from SM production and decay of the W boson, with the template changing based on the input value of m_W. The templates are generated using a custom Monte Carlo simulation with m_W as an input to vary the shapes of the templates. Further details of construction of the templates are given in [4]. The measured distributions agree with the shapes of the templates using a binned likelihood analysis, as seen in Fig. 2.6.

The kinematic observables used to extract m_W provide complementary systematics. In the rest frame of the W boson, the lepton and neutrino from its decay are back-to-back. This causes the p_T of the lepton and neutrino to have sharp Jacobian peaks at $m_W/2$. The transverse mass, given by

$$m_T^2 = (E_T^\ell + E_T^{\text{miss}})^2 - (\vec{p}_T^{\,\ell} + \vec{p}_T^{\,\text{miss}})^2, \tag{2.13}$$

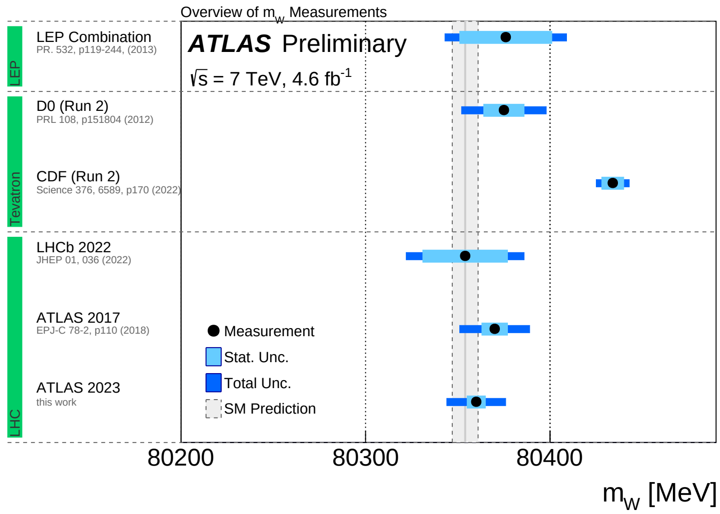

Figure 2.7: A comparison of the W boson mass measurements from LEP, Tevatron, and LH, taken from [3]. The total uncertainty of each measurement is shown in darker blue, with the precision of the measurements improving to $\sim 10 - 15$ MeV for the most recent results by CDF and ATLAS. The SM prediction via the electroweak fit is shown in the shaded gray vertical band. All but the CDF Run 2 measurement of m_W are consistent with the SM prediction, though CDF's measurement has the smallest uncertainty among them.

has a Jacobian peak at m_W. In the case of SM decay, $\vec{p}_T^{\,\text{miss}}$ is only the transverse momentum of the neutrino. However, these distributions undergo detector smearing, and the W bosons are not produced at rest in the lab frame. Initial state radiation (ISR) of gluons can boost the W bosons in the transverse direction in the lab frame. The measurement of p_T^ℓ is clean since it is not significantly affected by detector smearing, but it is sensitive to non-zero p_T^W. The effect of boosted W bosons in the sample can be mitigated by including a cut on the allowed hadronic recoil in the event, focusing on W bosons with minimal boost. On the other hand, the transverse mass m_T distribution is not shifted by nonzero p_T^W at leading order in QCD, but it is affected by detector smearing. Hence, m_T and p_T^ℓ provide complementary systematics [33].

To properly model the templates, a careful study of detector effects like smearing and pileup is required. The CDF collaboration in the supplemental material to [4] details the effects considered. Pileup, or "spectator interactions" as they are referred to in the CDF supplemental material, is the addition of soft processes recorded by the detector to the hadronic recoil which are not part of the parimary event which produces the W boson. Pileup effects are more significant for larger instantaneous luminosity since there are more bunch crossings. Ideally, low pileup runs would be used to mitigate pileup effects, but this strategy suffers from limited statistics.

Combining the results of the fits to these kinematic observables, CDF obtained a measured value of m_W = 80433.5 $\pm$ 9.4 MeV, the most precisely measured W boson mass to date to 0.01$\%$ uncertainty. This measurement is also in tension with the SM prediction from the EW fit of $m_W^{\text{pred.}}$ = 80354 $\pm$ 7 MeV, to 7σ statistical significance.

2.2.2 LHC Measurements of the W Boson Mass

In 2017, the ATLAS experiment at CERN published their Run-1 measurement of the W boson mass. ATLAS collects data from the Large Hadron Collider, which collides two proton beams at center-of-mass energy $\sqrt{s} = 7$ TeV for Run-1. The collaboration measured the W boson mass $m_W = 80370 \pm 19$ MeV with a dataset corresponding to an integrated luminosity $\mathcal{L} = 4.6$ fb^{-1}, containing ~ 14 million reconstructed W boson events after imposing all selection cuts [2].

Then in March 2023, ATLAS presented a remeasurement of the W boson mass, obtaining $m_W = 80360 \pm 16$ MeV, with a central value 10 MeV lower and 16% more precise than the 2017 measurement [3]. This updated measurement agrees with the SM prediction, unlike the CDF measurement.

There are a few notable differences between the ATLAS measurement and the CDF measurement. As mentioned earlier, the center-of-mass energy and statistics are higher for the AT-

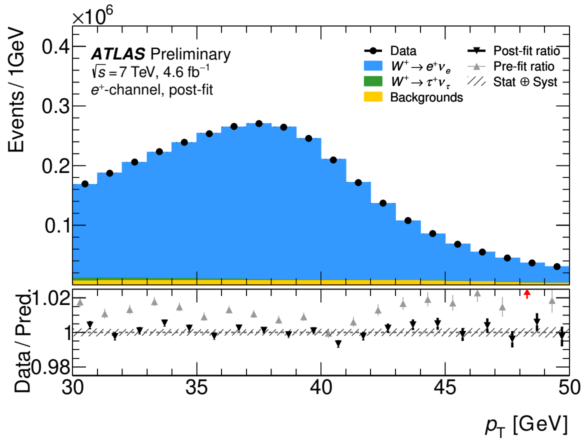

(a) p_T^ℓ fit, e^+ channel

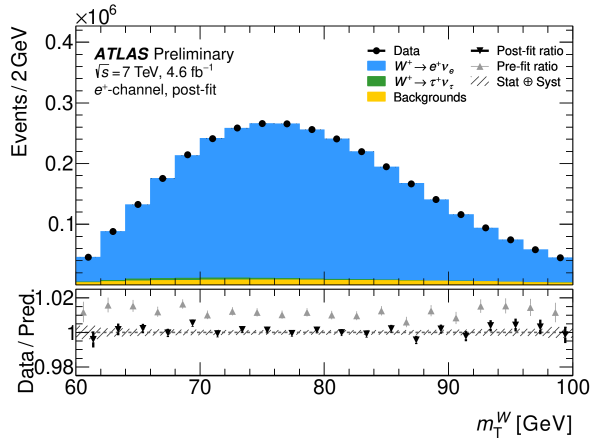

(b) m_T fit, e^+ channel

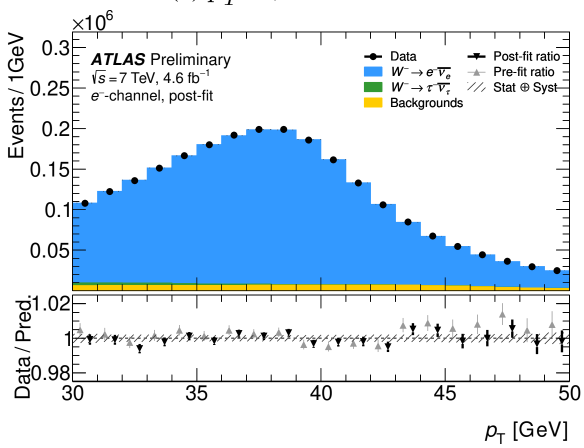

(c) p_T^ℓ fit, e^- channel

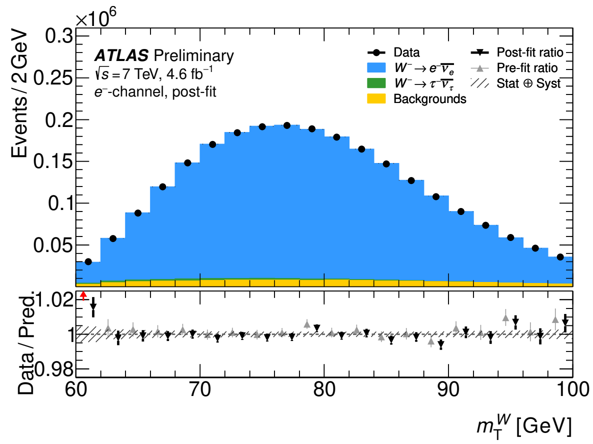

(d) m_T fit, e^- channel

Figure 2.8: Distributions of the kinematic observables p_T^μ, m_T for decays of $W^\pm$ to electrons.

LAS measurement as expected for the more recent LHC compared to the Tevatron. For selecting events, ATLAS imposes a different set of cuts, as summarized in Table 4.1. In particular, the ranges in p_T^ℓ and m_T are slightly different, but the biggest difference is the cut on hadronic recoil. CDF has a much tighter cut on hadronic recoil, only allowing events with recoil < 15 GeV, whereas ATLAS allows events with recoil < 30 GeV. This difference is in part due to the higher energies ATLAS accesses as well as higher pileup due to a larger instantaneous luminosity.

Additionally, ATLAS only uses p_T^ℓ and m_T kinematic distributions to extract m_W, whereas CDF includes p_T^ν. The fits of the templates to the data for electrons and muons are shown in

Figs. 2.8 and 2.9, respectively. In the lower panel of these distributions, ATLAS shows the combined statistical and systematic uncertainty across the kinematic regions to be $\lesssim 0.5\%$ per-bin uncertainty. This will motivate our choices of systematics considered in Chapter 4.

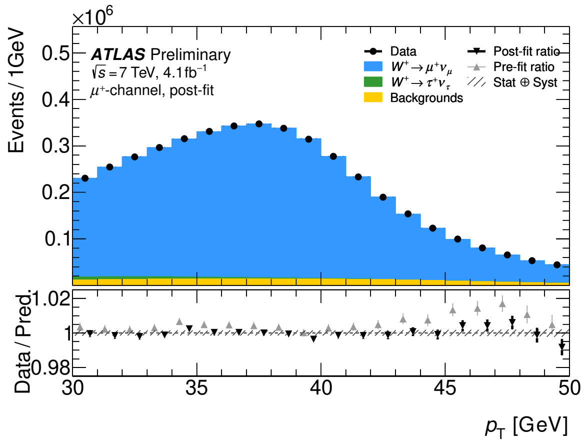

(a) p_T^ℓ fit, μ^+ channel

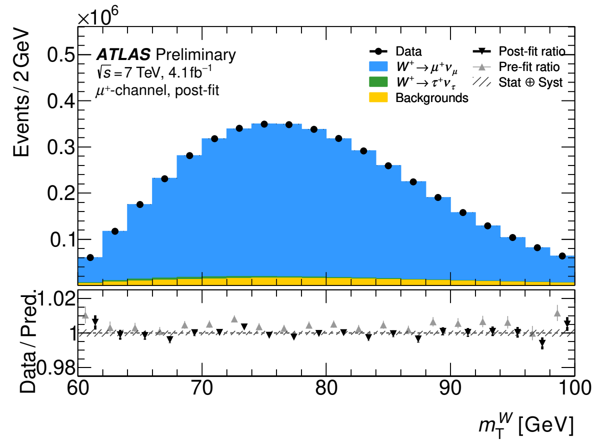

(b) m_T fit, μ^+ channel

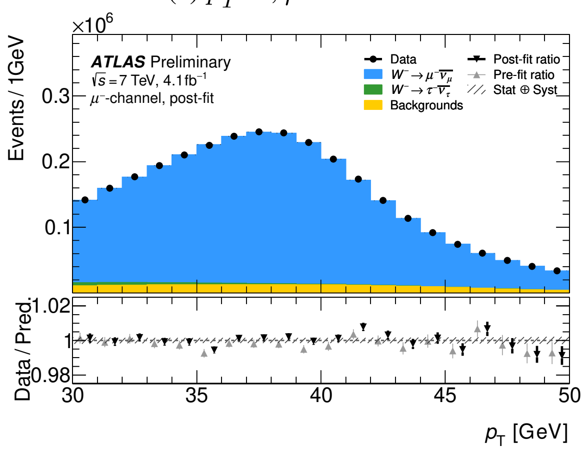

(c) p_T^ℓ fit, μ^- channel

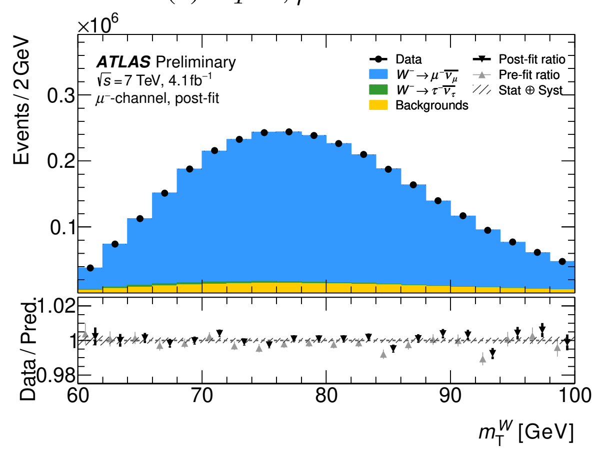

(d) m_T fit, μ^- channel

Figure 2.9: Distributions of the kinematic observables p_T^μ, m_T for decays of $W^\pm$ to muons.

Finally, while ATLAS has produced this remeasurement with better precision than their 2017 result and somewhat comparable precision to the CDF result, the collaboration has not yet produced a measurement of m_W with the Run-2 dataset, at higher center-of-mass energy and integrated luminosity. The CMS collaboration also has not yet announced a measurement of m_W, which could add more to the story. Hence, when discussing prospects of sensitivity to NP at the LHC, we will be referring to ATLAS.

2.3 A New Purpose for the W Boson Mass Measurement

With an understanding of how experiments measure m_W, we can now describe what kinds of new physics (NP) this measurement can probe, providing a new purpose for the W boson mass measurement. Since the final state of leptonic decay of the W boson is a charged lepton and a neutrino, appearing as missing transverse energy in the detector, any new physics which produces the same final state $\ell + \not{E}_T$ in the same kinematic region could contaminate the distributions used to measure m_W. However, since the measured distributions of the kinematic observables match the SM predictions of these distributions with great precision, any NP which modifies the shape of the kinematic distributions can be constrained.

There is a subtle point here regarding the tension between measurements of m_W by CDF and ATLAS. The SM prediction of the kinematic distribution depends on an input parameter, m_W, which is obtained from a fit to the measured distributions. Both CDF's and ATLAS's templates for the kinematic distributions agree with their respective extracted values of m_W, hence why either measurement can be used to probe direct effects of NP without any inconsistency.

The idea to probe new physics using precision measurements has been implemented before. For example, measurements of the top quark mass have been used to close the gap in searches for the supersymmetric stop, the superpartner of the top quark [34–36]. However, the precision of top quark mass measurements is not at the level of W boson mass measurement precision, at $\mathcal{O}(10^{-4})$, and the W mass measurement can be sensitive to NP charged only under electroweak interactions. We categorize the types of new physics and give examples of specific models we will consider in Chapter 3.

Chapter 3: Categorizing the New Physics Models

With the ability to probe light new physics using precision measurements of m_W, we now categorize the kinds of new physics that can produce the required $\ell + \not{E}_T$ final state. There are three categories of new physics which can be probed: (A) modified decay of the W boson, (B) modified production of the W boson, and (C) producing $\ell + \not{E}_T$ without an on-shell W boson. In the following sections, each of these categories will be described in more detail, with descriptions of specific examples of models which fit in each category and the relevant channels considered.

3.1 Modified W Decay

In this section, I will introduce the models under this category that we will probe using the m_W measurement. Since the W boson decays leptonically for the event selection considered by CDF and ATLAS for the most precise measurements of m_W, the modified decay NP models will coupled to charged leptons or neutrinos in some way. The examples of NP we consider are the $L_\mu - L_\tau$ Z' boson, neutrinophilic scalar ϕ, and heavy neutrino ν_4.

3.1.1 $L_\mu - L_\tau$ Leptophilic Z' Model

The first model that we consider is the $L_\mu - L_\tau$ leptophilic Z' [37]:

$$\mathcal{L}_{\text{int}} = g_{Z'} Z'_\rho J^\rho_{\mu-\tau} + g_D Z'_\rho J^\rho_D \,, \tag{3.1}$$

where $g_{Z'}$ and g_D are the couplings of Z'-boson to SM and dark-sector states, respectively. The $U(1)_{L_\mu - L_\tau}$ current reads

$$J^\rho_{\mu-\tau} \;=\; (\bar{\nu}_\mu \gamma^\rho \nu_\mu + \bar{\mu}\gamma^\rho \mu - \bar{\nu}_\tau \gamma^\rho \nu_\tau - \bar{\tau}\gamma^\rho \tau). \tag{3.2}$$

The term $Z'_\rho J^\rho_D$ describes the interaction of the Z'-boson with some invisible, unspecified dark-sector states. The key assumptions, that $g_D \gg g_{Z'}$ and the dark sector contains states sufficiently lighter than $m_{Z'}$, guarantee that the Z'-boson decays predominantly invisibly.

This model has been extensively studied as a possible portal to dark matter or as an extension to SM. The 2-dimensional parameter space $(g_{Z'}, m_{Z'})$ is tested by a variety of searches, from K-/B-factories, $g-2$, to neutrino beam-dump experiments [10, 38].[1] In this model belonging to category (A), the W-boson has a 3-body decay into $\mu\,\nu_\mu\,Z'$ (Fig. 3.1), modifying the kinematic distributions of $\ell + \not{E}_T$ final state.[2]

[1] Additional constraints arise when $m_{Z'}$ is of Stueckelberg origin [39].

[2] Additional signal events come from $\tau \to Z' \mu\, \nu_\mu\, \nu_\tau$. For simplicity we don't include them in our analysis.

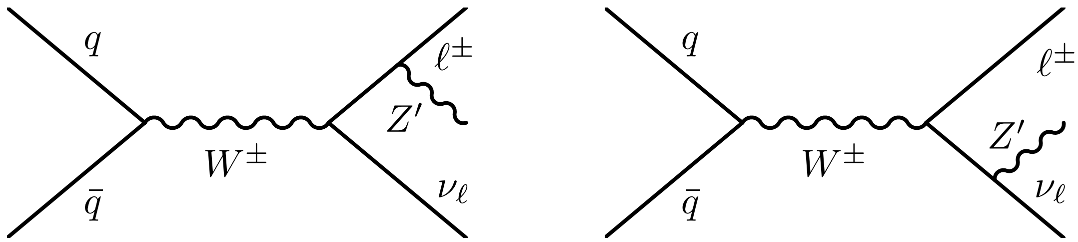

Figure 3.1: Feynman diagrams of modified W boson decay with a leptophilic Z' boson.

3.1.2 Neutrinophilic Scalar ϕ Model

Another example of modified decay that we study is the "neutrinophilic" scalar model of [11, 40, 41]. Neutrinophilic mediators are well-motivated messenger particles that can probe some of the least known sectors of fundamental physics involving nonstandard interactions of neutrinos with themselves and potentially with dark matter. The new ingredient of this model is an effective interaction between the SM and a new "invisible" scalar ϕ of the form

$$\mathcal{L} \supset \frac{c_{\alpha\beta}}{\Lambda^2}\,(L_\alpha H)\,(L_\beta H)\,\phi\,. \tag{3.3}$$

This new particle ϕ is a SM singlet with mass M_ϕ and it is assumed to be lighter than the Higgs boson. At low energies, after electroweak symmetry breaking, Eq. (3.3) produces a new interaction between the SM neutrinos and this new scalar

$$\mathcal{L}_{\text{int}} \supset \sum_{\alpha,\beta=e,\mu,\tau} \frac{1}{2}\lambda_{\alpha\beta}\nu_\alpha\nu_\beta\phi\,, \tag{3.4}$$

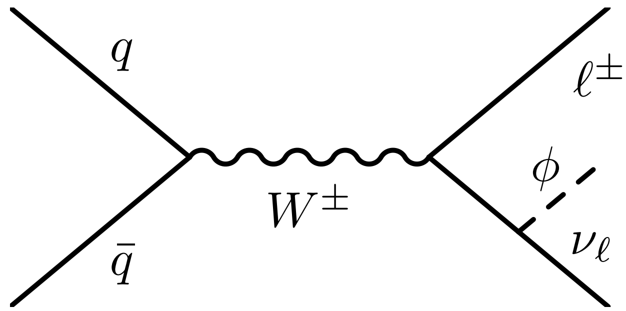

Figure 3.2: Feynman diagrams of modified W boson decay with a neutrinophilic scalar boson ϕ.

where $\lambda_{\alpha\beta}$ parameterizes the effective coupling of ϕ to neutrinos. In fact, Eq. (3.4) opens the new decay channel via radiative emission of ϕ from ν

$$W \to \ell\,\nu^* \to \ell\,\nu\,\phi\,. \tag{3.5}$$

Since ϕ is invisible by construction, this decay mode gives $\ell + \not{E}_T$ (see Fig. 3.2), directly affecting the W boson mass measurement.

We refer to [11, 40, 41] for any general aspects of the phenomenology and the modeling of this scenario. Here, we simply focus on the sensitivity of the W boson mass measurement to the interaction in Eq. (3.4).

3.1.3 Heavy Neutrino ν_4 Model

Another scenario to which our sub-electroweak new physics search strategy is sensitive is the so-called "heavy neutrino" scenario [42]. The main novelty is that the *three* active SM neutrinos in the flavor basis are a linear combination of *four* mass eigenstates, that we denote $\nu_{1,2,3}$ for the massless neutrinos and an additional sterile "heavy" neutrino ν_4 of mass m_{ν_4}. The

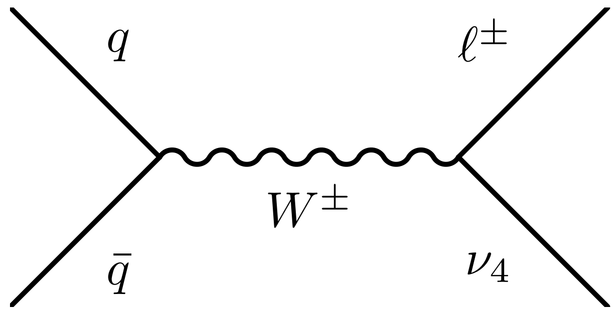

Figure 3.3: Feynman diagram of modified W boson decay with a heavy neutrino ν_4.

active neutrinos are defined as superpositions

$$\nu_\alpha = \sum_{i=1}^{4} U_{i\alpha}\nu_i\,, \qquad \text{for} \qquad \alpha = e,\ \mu,\ \tau\,. \tag{3.6}$$

This framework is typical, for instance, of models where the heavy neutrino acts as the portal to the dark sector [12, 43]. We do not elaborate on this aspect any further and instead focus on the collider phenomenology of models of this sort. The following interactions induced by the mixing in Eq. (3.6) are of interest

$$\mathcal{L}_{\text{int}} \supset \sum_{\ell=e,\mu,\tau} U_{4\ell} W_\mu^+ \bar{\nu}_4 \gamma^\mu \ell_L^- + \text{h.c.}\,. \tag{3.7}$$

Assuming that the heavy neutrino is effectively invisible, one can see that the above interactions allow an anomalous W decay (see Fig. 3.3)

$$W \to \ell\,\nu_4\,, \tag{3.8}$$

which contributes to the $\ell + \not{E}_T$ final state.

One interesting aspect of the heavy neutrino scenario which differentiates it from the other

NP models in the modified decay category is the 2-body decay like the SM process, but now to a massive invisible particle. It is still expected to produce a softer lepton spectrum, though not necessarily in the same way that a 3-body decay would.

3.2 Modified W Production

3.2.1 $U(1)_B$ Hadrophilic Z' Model

As an example of anomalous W boson production, we consider the case of the so-called hadrophilic Z', i.e., a new gauge boson coupled to the baryon number. The effective interaction is described by

$$\mathcal{L}_{\text{int}} = g_{Z'_B} \bar{q} \not{Z}'_B q \,, \tag{3.9}$$

with q spanning over all the SM quarks.[3] We denote the mass of this additional gauge boson by $M_{Z'_B}$. Interactions of the Z'_B of this form have been widely studied in the literature, either in the context of a simple extension to the SM or as a possible portal to dark matter (see for instance [44, 46–49] and references therein). Like the previous models, we only focus on the collider phenomenology of Eq. (3.9), under the assumption that the Z'_B or its decay products do not leave observable traces in collider experiments, hence the Z'_B contributes to the $\not{E}_T$.

This model belongs to category (B), since the SM W boson can be produced in association

[3] We remark that as the baryon number has an anomalous current, Eq. (3.9) is to be understood only as effective theory supported by an additional Wess-Zumino term. As pointed out, for instance, in [44], this may lead to very strong constraints. Yet these effects are not completely model-independent, as discussed, for instance, in [44, 45], and we, therefore, do not pursue any further discussion.

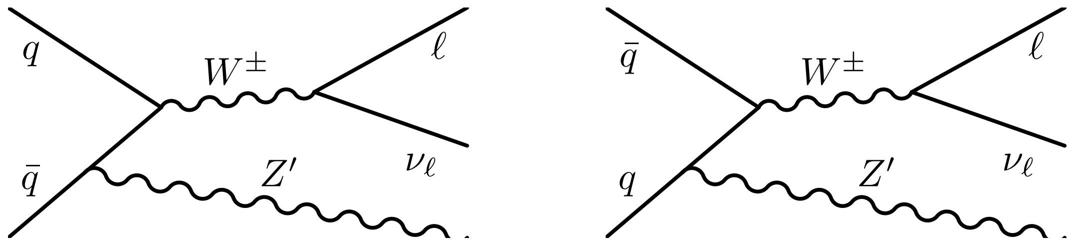

Figure 3.4: Feynman diagrams of modified W boson decay with a hadrophilic Z' boson.

with this gauge boson as shown in Fig. 3.4:

$$pp \to W(\ell\nu)\, Z_B^{'}\,,$$

which produces a $\ell + \not{E}_T$ signature.

3.3 $\ell + \not{E}_T$ without an on-shell W

The final category of models we consider is rather broad, considering the production of $\ell + \not{E}_T$ without the inclusion of an on-shell W boson. Many models can produce such a signal, from Standard Model Effective Field Theory (SMEFT) operators of a heavy W' boson to slepton-sneutrino production in the Minimal Supersymmetric Standard Model (MSSM). Here I'll briefly discuss the different kinds of models in this category before introducing in more detail the MSSM.

Similar to the Z' models already discussed, there are ongoing searches for a W' boson, though usually at higher energy scales than the SM W boson. These kinds of searches are looking for signs of SMEFT operators at high energy with $\ell + \not{E}_T$ final state [23]. Some concrete examples of models which predict a heavy W' boson are extra dimensional models predicting a Kaluza-Klein mode of the W, or in R-Parity-Violating (RPV) supersymmetry, a τ slepton.

Searches for heavy W' bosons are performed in the tails of the kinematic distributions, and therefore do not have much overlap with the measurement of m_W. However, other models producing $\ell + \not{E}_T$ can produce signals near the Jacobian peak of the SM W. For this purpose, we will be focusing on slepton-sneutrino production in the MSSM, whose kinematic distributions of the lepton in the compressed region of the parameter space mimics that of the lepton emitted by the SM W boson.

3.3.1 The Minimal Supersymmetric Standard Model: Slepton-Sneutrino Production

Supersymmetry (SUSY) is a theoretical framework in particle physics that extends the SM, aiming to address several of its limitations. It was arguably one of the most popular extensions to the SM due to its ability to solve the hierarchy problem and provide a dark matter candidate by introducing a new symmetry between bosons and fermions. SUSY posits that every fundamental particle in the SM has a corresponding superpartner with differing spin properties. Specifically, for each boson, there exists a fermion superpartner and vice versa through the following supersymmetric transformation [50–54]:

$$Q|\text{Boson}\rangle = |\text{Fermion}\rangle,\ \text{Q}|\text{Fermion}\rangle = |\text{Boson}\rangle. \tag{3.10}$$

For example, the superpartner of the charged leptons (fermions) are “sleptons”, and the superpartner of a photon (boson) is a photino (fermion). For a review, see [55, 56].

One of the main motivations for introducing the superpartners is to solve the Planck-weak hierarchy problem, which involves the large discrepancy between the electroweak scale and the Planck scale, where gravitational effects become significant. Without SUSY, the Higgs boson

Particles/superparticles		spin 0	spin 1/2	$SU(3)_C \times SU(2)_L \times U(1)_Y$
leptons, sleptons	(L)	$(\widetilde{\nu}, \widetilde{e}_L)$	(ν, e_L)	$(1, 2, -1/2)$
(in 3 families)	(E^c)	$\widetilde{e}^*_R$	e^c_L	$(1, 1, 1)$
quarks, squarks	(Q)	$(\widetilde{u}_L, \widetilde{d}_L)$	(u_L, d_L)	$(3, 2, 1/6)$
(in 3 families)	(U^c)	$\widetilde{u}^*_R$	u^c_L	$(\bar{3}, 1, -2/3)$
	(D^c)	$\widetilde{d}^*_R$	d^c_L	$(\bar{3}, 1, 1/3)$
Higgs, higgsinos	(H_u)	(H^+_u, H^0_u)	$(\widetilde{H}^+_u, \widetilde{H}^0_u)$	$(1, 2, 1/2)$
(up, down types)	(H_d)	(H^0_d, H^-_d)	$(\widetilde{H}^0_d, \widetilde{H}^-_d)$	$(1, 2, -1/2)$
Particles/superparticles		spin 1	spin 1/2	$SU(3)_C \times SU(2)_L \times U(1)_Y$
gluon, gluino		g	$\widetilde{g}$	$(8, 1, 0)$
W bosons, winos		$W^\pm, W^0$	$\widetilde{W}^\pm, \widetilde{W}^0$	$(1, 3, 0)$
B boson, bino		B^0	$\widetilde{B}^0$	$(1, 1, 0)$

Table 3.1: A table of the particle content of the MSSM. Superpartners are marked by a "tilde" over the particle. This table was taken from [1].

mass would require fine-tuning to remain at the observed value since there are large quantum corrections to m_H^2 from any particles that couple to the Higgs. Notably, the Higgs mass is quadratically sensitive to high mass scales, so regularization of quadratic divergences does not alone solve the hierarchy problem. The addition of superpartners helps stabilize the Higgs mass through the loop contributions of superpartners, canceling out the quantum corrections to keep the Higgs mass small.

The Minimal Supersymmetric Standard Model (MSSM) is the simplest extension of the SM that incorporates SUSY. It introduces the minimal number of new particles and interactions required to include SUSY, aiming to address the same issues as SUSY while remaining as close as possible to the SM [56]. The particle content of the MSSM is shown in Section 3.3.1.

Additionally, the MSSM provides a potential candidate for dark matter. This is achieved through R-parity, which distinguishes SM particles from their superpartners. SM particles have R-parity +1, while the superpartners have R-parity -1. The conservation of R-parity implies that the lightest supersymmetric particle (LSP) is stable. In many scenarios, it also interacts weakly with regular matter, fitting the profile of dark matter particles. The LSP is often a neutralino, which is a mixture of the superpartners of the photon, Z boson, and neutral Higgs bosons.

Thus far it has been assumed that the superpartners have the same properties as their SM counterparts except for their spin. However, if this was the case, the superpartners would have already been discovered. Therefore, supersymmetry must be broken in such a way that the superpartners are much heavier than their SM counterparts. Naively one would think that since the Large Hadron Collider has reached $\sim$ 13 TeV center-of-mass energy that all superpartners have been ruled out to multi-TeV mass scales, but there are gaps in searches for some superpartners because there are regions of parameter space where the SM background is dominant. This is the region where a unification of searches for MSSM with measurements of SM observables could be sensitive to the effects of new physics.

There are many additional details of the MSSM such as gauge coupling unification at high energies, two Higgs doublets instead of one as in the SM, etc., but the main focus is on how the MSSM can produce a signal which W boson mass measurements can probe. For that, the important interactions in the MSSM are slepton-sneutrino production through an off-shell W boson and the slepton decays to a SM lepton and a neutralino $\tilde{\chi}_1^0$ and the sneutrino $\tilde{\nu}$. The full processes are shown in Fig. 3.5 for two scenarios: Fig. 3.5a shows when the neutralino is the LSP, and Fig. 3.5b shows when the sneutrino is the LSP.

Additionally, there are other SUSY scenarios which produce $\ell + \not{E}_T$ exist without requiring

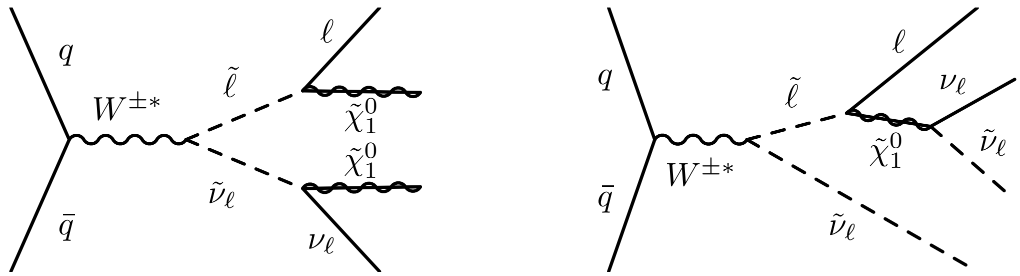

(a) Neutralino as LSP (b) Sneutrino as LSP

Figure 3.5: Feynman diagrams of MSSM slepton-sneutrino production, leading to a $\ell + \not{E}_T$ final state.

the MSSM relation between slepton and sneutrino mass, for example [57], where the sneutrino is the LSP. In this model, the neutralino can be very heavy, forbidding the process in Fig. 3.5a and suppressing channels like Fig. 3.5b, but allowing for the slepton to decay to sneutrino and W boson, which decays leptonically: $\tilde{\ell} \to \tilde{\nu}_\ell W \to \tilde{\nu}_\ell \ell \nu_\ell$. The difficulty in probing such a process comes from the effective 3-body decay of the slepton. The softer spectrum of the lepton from 3-body decay in this process vs. 2-body decay in Fig. 3.5a reduces the sensitivity to such signals since, as shown later, the MSSM processes modify the kinematics above the Jacobian peak of the W boson.

3.4 Search Strategies for New Physics

In this current approach by experiments, shown in Fig. 1.1, searches and measurements are separated in the phase space of measured distributions. SM measurements are at lower energies using precisely measured distributions with sub-percent systematics. With this strategy, searches for new physics at high energy colliders are not sensitive to light NP. If the NP sensitivity is dominant in the SM-rich region, then a unification of searches and measurements is required to probe such NP. This is what we propose in the sub-electroweak and circa-electroweak regions in

Fig. 1.2.

The sub-EW and circa-EW strategies are independent of the electroweak fit prediction of m_W, and they are not the usual SMEFT approach of probing effects of heavy NP. These models described above would directly affect the measured sample used to extract m_W. Thus we also do not consider any supra-EW analyses, since these are the usual W' searches already done by CMS [23]. Furthermore, while the NP models described could affect the EW fit prediction of m_W, this does not change our ability to be sensitive to these models from measurements of m_W alone.

In the following chapters, I will describe in more detail the search strategies for the sub- and circa-electroweak analyses, and provide sensitivity projections for each of the models compared to the current strongest constraint on each model.

Chapter 4: Sub-Electroweak Analysis

We now focus on searching for new physics with $\ell + \not{E}_T$ final state whose sensitivity is near the region used to measure m_W. Thus a proper analysis requires unifying the search for new physics with the measurement of m_W, resulting in a simultaneous fit of SM and NP parameters. The chapter begins with an overall description of the analysis in this kinematic region. In particular, details of the binned likelihood shape analysis are provided, as well as the general prescription applied to each model.

4.1 A general overview of the Sub-Electroweak Analysis

As to profit as much as possible from measurements that have been *already* carried out, we choose the distribution of lepton p_T^ℓ and the transverse mass m_T of the $\ell+\not{E}_T$ system for our LHC projections. We take as reference the W boson mass measurements from ATLAS [2,3]. For CDF projections, we also include the missing transverse momentum p_T^{miss} distribution, as it was done by the experiment itself in their W boson mass measurement [4]. As pointed out in [58], there is a remarkable interplay between new physics searches and SM measurements, so much so that the two must be considered part of the same analysis. Concretely, this entails that the interpretation of the data in these models requires the simultaneous fit of m_W and the new physics parameters. Analogously, a fair SM measurement for m_W should take into account possible BSM effects as nuisance parameters in the likelihood.

We thus construct a χ^2 for each model and for each binned distribution of the observable $\mathcal{O}$:

$$\chi^2_{\mathcal{O}}(\Delta_{m_W}, \theta_{\rm NP}) = \sum_{i,\, j=1}^{N_{\rm Bins}} \left(N^i(\Delta_{m_W}, \theta_{\rm NP}) - \overline{N}^i \right) \Sigma^{-1}_{ij} \left(N^j(\Delta_{m_W}, \theta_{\rm NP}) - \overline{N}^j \right) \,, \tag{4.1}$$

where $\bar{N}_i$ is the observed and $N^i(\Delta_{m_W}, \theta_{\rm NP})$ is the expected number of events for observable $\mathcal{O}$ in the the bin i as function of m_W. In the sub-EW region, following experimental procedure, the distributions are normalized, meaning the number of events predicted by the template N_i will match the number of events in the data $\bar{N}_i$. Hence, the χ^2 calculated is sensitive to the $shape$ of the distribution of the template, unlike a typical cut-and-count search for new physics. The actual value of m_W will not matter, since we track the m_W dependence in our calculations through the mass difference $\Delta_{m_W} = m_W - \overline{m}_W$, where $\overline{m}_W$ is the W mass in the MC sample we use as substitute for the data from the actual experiment. Notably our χ^2 depends and the NP parameters θ_{NP}, whose nature will differ for each model we will consider in the following. Here, Σ^{-1}_{ij} denotes the inverse of the covariance matrix Σ_{ij} including various uncertainties

$$\Sigma_{ij} = \Sigma^{\rm stat}_{ij} + \Sigma^{\rm unc}_{ij} + \Sigma^{\rm cor}_{ij} \,. \tag{4.2}$$

The first term accounts for the statistical uncertainties while the second and the third terms model the systematic uncertainties through completely uncorrelated and completely correlated components, respectively, common for all the bins:

$$\Sigma^{\rm stat}_{ij} = \overline{N}^i \delta_{ij} \,, \qquad \Sigma^{\rm unc}_{ij} = (\overline{N}^i \epsilon^{\rm unc})^2 \delta_{ij} \,, \qquad \Sigma^{\rm cor}_{ij} = \overline{N}^i \overline{N}^j (\epsilon^{\rm cor})^2 \,, \tag{4.3}$$

where δ_{ij} is the usual Kronecker delta while $\epsilon^{\rm unc}$ and $\epsilon^{\rm cor}$ are fractional factors parameterizing the uncorrelated and correlated systematics, respectively. The pseudo-data sets are generated assuming the SM with W-boson mass $\overline{m}_W$, hence the χ^2 is minimized at $\Delta_{m_W} = \theta_{NP} = 0$.

We will perform two different types of analyses targeting sub-electroweak scale new physics or circa-electroweak scale new physics. For these targets we will adopt, respectively, two baseline analysis setups: i) the sub-electroweak analysis described in Chapter 4, in which we try as much as possible to study distributions obtained under event selection closely following the ATLAS and CDF W boson mass measurements; ii) the circa-electroweak analysis, described in Chapter 5, in which we allow for larger deviations in the event selection, and in particular in the range of $p_{T,\ell}, m_T$ and $p_T^{\rm miss}$, as to maximize the reach in the search for new physics.

All our LHC projections are based on Monte Carlo (MC) simulations produced via MADGRAPH5_AMC@NLOv3.42 [59] + PYTHIA8.212 [60] + DELPHESv3.4 [61] (ATLAS card). Regarding the parton distribution functions (PDFs), we employ LHAPDF [62] with PDF ID:244800 [63]. Pileup of collisions, with average number of pileup events per bunch crossing $\langle\mu\rangle$ = 50, is simulated through the dedicated DELPHES ATLAS card. In our results, pileup is always included unless indicated otherwise. For the CDF projections, we simulate detector effects through a custom MC code package, implementing the results of [4] (see the Appendix of Ref. [58] for details). The rest of the CDF setup matches what is done for the LHC. For concreteness, we only simulate the cases resulting in muons in the final state. Nevertheless, we expect that completely analogous results will apply to the cases involving electrons in the final state. In the following we analyze the muon final state without performing any combination with the electron final state, unless noted otherwise.

We do not include any backgrounds to the W boson mass measurement in the χ^2 of

Eq. (4.1) because these backgrounds can be estimated from MC and are only a few percent [2–4] of the SM W boson events in our analysis range. Indeed, for our analyses in the sub-electroweak region (in Section 4.2 and Section 4.3), we consider analysis ranges similar to those of ATLAS [2,3] and CDF [4]; we slightly enlarge the ranges to maximize the sensitivity to new physics, as shown in Table 4.1). On the other hand, for our analysis in Section 5.1, we substantially modify the analysis range from the W-boson mass measurement to the circa-electroweak region. However, even in this case, we expect backgrounds to be only marginally relevant, as we comment in detail in Section 5.1.

As shown from the kinematic distributions and the associated S/B ratios in Figs. 4.1 and 4.5, a great deal of the sensitivity to new physics comes from the p_T and m_T spectra near the SM Jacobian peak [5]. Therefore, we design our analysis as much as possible around the currently published W-boson mass measurements [2–4]. For reference we give in Tab. 4.1 a summary of the event selection used for the current measurements of the W boson mass and in our sub-electroweak analysis.

For the sub-electroweak analyses, we only use the shape of the distribution for the search of new physics and the simultaneous determination of m_W. The same approach is used by ATLAS in their W mass measurements. Therefore we normalize the expected number of events N_{ev}^i in Eq. (4.1) to the pseudo-data in each computation of the χ^2 between pseudo-data and the expected distribution. Because of this normalization, we do not include any correlated components in the systematics (i.e., $\epsilon^{\text{cor}} = 0$). For the uncorrelated components, we consider a few benchmark scenarios; we consider $\epsilon^{\text{unc}} = 0\%, 0.1\%$, and 0.5% for the LHC projections and $\epsilon^{\text{unc}} = 0\%$ and 1% for the CDF ones.

	p_T^ℓ	$p_T^{\rm miss}$	m_T	$\lvert\vec{u}_T\rvert$	m_T range	p_T^ℓ range
ATLAS [2, 3] ($W \to \mu\,\nu_\mu$)	> 30 (analysis) > 18 (trigger)	> 30	> 60	< 30	$[60, 100]$	$[30, 50]$
Sec. 4.2.1 ($W \to \mu\nu_\mu Z'$)	> 20	> 20	> 40	< 30	$[40, 100]$	$[20, 50]$
Sec. 4.2.2 ($W \to \mu\nu_\mu\phi$)	> 20	> 20	> 40	< 30	$[40, 100]$	$[20, 50]$
Sec. 4.2.3 ($W \to \mu\nu_4$)	> 20	> 20	> 40	< 30	$[40, 100]$	$[20, 50]$
Sec. 4.3 ($pp \to WZ'$)	> 30	> 30	> 60	< 30	$[60, 140]$	$[30, 70]$
Sec. 4.4 ($pp \to \tilde{\ell}\tilde{\nu}$)	> 30	> 30	> 60	< 30	$[60, 120]*$ $[60, 140]$	$[30, 60]*$ $[30, 70]$
CDF (μ) [4]	$[30, 55]$ (analysis) > 18 (trigger)	$[30, 55]$	$[60, 100]$	< 15	$[65, 90]$	$[32, 48]$
Sec. 4.2.1 ($W \to \mu\nu_\mu Z'$)	$[20, 55]$	$[20, 55]$	$[60, 100]$	< 15	$[40, 90]$	$[20, 48]$
Sec. 4.2.2 ($W \to \mu\nu_\mu\phi$)	$[20, 55]$	$[20, 55]$	$[60, 100]$	< 15	$[40, 90]$	$[20, 48]$
Sec. 4.2.3 ($W \to \mu\nu_4$)	$[20, 55]$	$[20, 55]$	$[60, 100]$	< 15	$[40, 90]$	$[20, 48]$

Table 4.1: Kinematic cuts and analysis ranges considered in the latest W-mass measurements [2–4] and in our sub-EW analyses. All the numbers are in units of GeV. The hadronic recoil vector is denoted by $\vec{u}_T$. For our LHC projections, we construct 2 GeV bins for m_T and 1 GeV bins for p_T^ℓ [3], unless otherwise specified. For the CDF projections, we construct 0.5 GeV bins for m_T and 0.25 GeV bins for p_T^ℓ, $p_T^{\rm miss}$ [4]. The analysis ranges of p_T^ℓ apply also to $p_T^{\rm miss}$ in the CDF analyses.

4.2 Probing Modified W Decay in the Sub-EW Region

In this section, we focus on probing NP modifying the W boson decay. In two of the scenarios presented, the modified decay is now a 3-body decay, which softens the lepton transverse momentum distribution compared to the 2-body decay in the SM. This softening of p_T^ℓ motivates a sub-electroweak analysis as the sensitivity to NP will be below the Jacobian peak.

4.2.1 $L_\mu - L_\tau$ Leptophilic Z'

The first model we consider is the $L_\mu - L_\tau$ leptophilic Z', which couples to muons and taus. This model is motivated theoretically as one of the possible gauge-anomaly-free symmetries in the SM. Details of the model specifics are provided earlier in Section 3.1.1. The softer p_T and m_T distributions of the NP, as seen in Fig. 4.1 for a benchmark value of $(m_{Z'}, g_{Z'}) = (10\,\mathrm{GeV}, 0.12)$.[1]

[1]NP also modifies W-boson total decay width. This effect is expected to be negligible given the projected bound on the NP parameters. Therefore we fix the width to its SM value. The effect of the width on the m_W determination

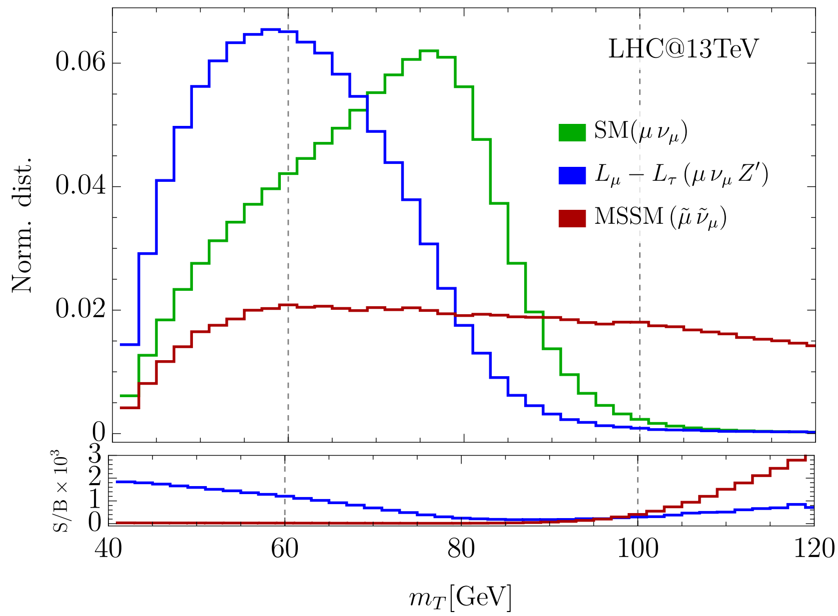

Figure 4.1: Normalized transverse mass distributions for $\mu + \not{E}_T$ at the LHC. Blue line: $m_{Z'} = 10\,\mathrm{GeV}, g_{Z'} = 0.12$). Red line: $m_{\tilde{\mu}} = 115\,\mathrm{GeV}$, $m_{\tilde{\nu}} = 83\,\mathrm{GeV}$, $m_{\tilde{\chi}_1^0} = 70\,\mathrm{GeV}$. The dashed gray lines indicate the ATLAS analysis region of m_T used to measure m_W.

As shown in Fig. 4.1, for $g_{Z'} \sim \mathcal{O}(0.1)$, the expected S/B ratio is $\mathcal{O}(10^{-3})$. Sensitivity to these effects strongly relies on the various sources of uncertainties, which is exactly the main target for the experimental collaborations that reached percent [4] and even sub-percent uncertainties [2, 3], aimed at measuring m_W. Also backgrounds are extensively studied and they are only a few% in the region of interest. In this letter we will not attempt a complete study of the various sources of uncertainties in the presence of NP. We just comment on the possible effect of our NP hypothesis on the sample of $Z \to \ell\ell$ events which are heavily used for detector calibration [2, 4] and for tuning the boson production model on data [64]. Thus a contamination of NP in the $Z \to \ell\ell$ sample might affect the calibration of the MCs, "calibrating away" signs of NP [65]. However, by isolating pure Z-boson events with appropriate kinematic cuts, such as those imposed by ATLAS [2]: $80 < m_{\ell\ell}/\mathrm{GeV} < 100$, the possible contamination of NP in the

within the SM is only a few MeV. [3, 64].

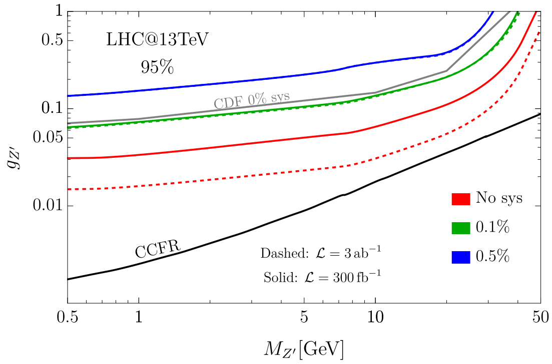

(a) $pp \to \mu\,\nu_\mu\,Z'$

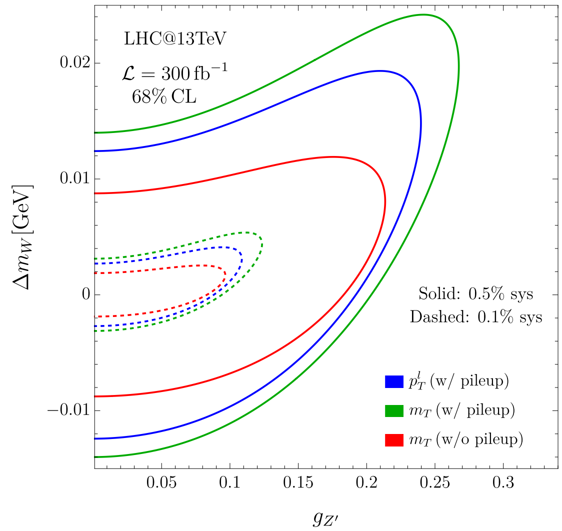

(b) $pp \to \tilde{\mu}\,\tilde{\nu}_\mu$

Figure 4.2: LHC 95% CL projected sensitivity to (a) $L_\mu - L_\tau$. All the lines include detector simulations. Pileup ($\langle\mu\rangle = 50$), simulated through the dedicated DELPHES ATLAS card, is included unless indicated otherwise. Present bounds are obtained from [10].

calibration sample is limited to $\mathcal{O}(10^{-4})$, still for $g_{Z'} \sim \mathcal{O}(0.1)$.

We estimate the sensitivity and the impact of our NP hypothesis on the m_W measurement through a binned χ^2 analysis for the p_T^ℓ and m_T distributions. Our analysis is aligned as much as possible with the ATLAS measurement [2, 3], only slightly extending the fit range aiming at maximal sensitivity, shown in Table 4.1. We then compute the χ^2 as shown in Section 4.1. We stress that we are testing the New Physics hypothesis with no prior on $\overline{m}_W$, as both Δ_{NP} and m_W are floated.

On the contrary, the authors of [66] *fixed* m_W in the hypothesis to the EW fit prediction. The simultaneous fit to m_W and NP that we perform here is thus a more general test of NP and has the added value to be independent of the EW fit results and the assumptions therein.

The qualitatively new aspect of Δ_{m_W} being a floated parameter in Eq. (4.1) implies that with the same analysis we extract m_W and test NP. The 2-dimensional fit in the $(\Delta_{m_W}, \Delta_{\text{NP}})$ is reported in Fig. 4.2b for $m_{Z'} = 10$ GeV. By assuming 0.5% per-bin uncorrelated systematics and including the effect of pileup through DELPHES, the ATLAS measured uncertainty is roughly reproduced.[2] Pileup has an impact on the m_T distribution and on the resulting m_W sensitivity. The p_T^ℓ distribution, on the contrary, is largely insensitive to pileup, hence we use it to draw more firm conclusions on features of our 2D-fit.

The systematics on the kinematic distributions shown in [3] are below 0.5%. Therefore, we also consider per-bin systematics of 0.1%. The expected sensitivity to m_W (at zero $g_{Z'}$) is slightly stronger than the current ATLAS 7 TeV $\mathcal{L} = 4.6$ fb^{-1} measurement [3]. This is mainly because we are not including any source of correlated systematics, and we are assuming much larger statistics from a 13 TeV run with $\mathcal{L} = 300$ fb^{-1}.

The distortion of the p_T^ℓ exclusion line (blue) at large values of $g_{Z'}$ implies a preference towards positive Δ_{m_W}. This suggests that NP might in principle impact the sensitivity to m_W, possibly producing a shift in the extracted value and/or affecting the estimate of the associated uncertainty on m_W. Yet, the effect shown in Fig. 4.2b is limited to only ~ 10 MeV. However, a quantitative assessment of this effect requires the inclusion of the proper experimental setup and is beyond the scope of this letter. The sensitivity to $g_{Z'}$ at $\Delta_{m_W} = 0$ is only marginally affected by pileup, showing the robustness of the sensitivity to NP.

For completeness, we report in Section 4.2.1.1 an analogous study for CDF [4]. In this case, the effect of the NP in the m_W determination is less pronounced, due to a sharper Jacobian peak related to the better control of the hadronic activity at CDF which anchors the m_W fit more robustly. However, the sensitivity to NP is statistics-limited, with no prospect for improvements as CDF is no longer collecting data.

[2] The average number of pileup events per bunch crossing is $\langle \mu \rangle = 50$.

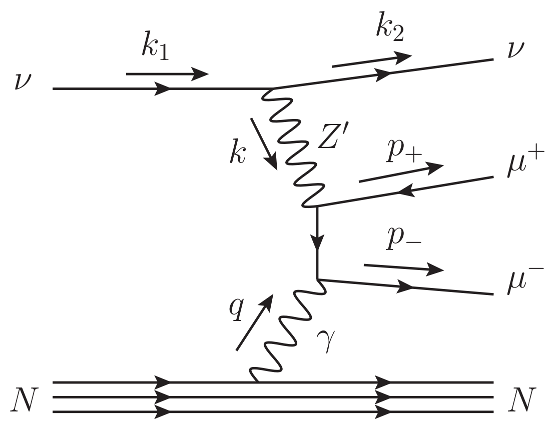

Figure 4.3: Feynman diagram of the neutrino trident production via Coulomb interactions probed by the CCFR experiment. The diagram is taken from [10].

We now turn to the test of the NP hypothesis. Assuming no prior knowledge on $\overline{m}_W$, the correct procedure to put bounds on NP is to marginalize on Δm_W for each value of the NP parameters. This is shown in Fig. 4.2a for LHC ($\mathcal{L} = 300$ fb^{-1}) sensitivity projection. Prior knowledge on $\overline{m}_W$ (either from other measurements or from theory predictions) might impact the sensitivity to NP, as shown in Fig. 4.2b.

For this analysis, positively and negatively charged-muon events are added together, and χ^2 for p_T^ℓ and m_T are combined without correlation. Here, the sensitivity projections for CDF are also reported. The reach for $m_{Z'} \simeq 10$ GeV is competitive with the best probe for this model from a dedicated experiment: Chicago-Columbia-Rochester-Fermilab (CCFR) [10, 67]. The experiment probes neutrino trident production through Coulomb interactions, as shown in Fig. 4.3.

Yet, it is remarkable that for a 10 GeV Z'-boson, the m_W measurement has the power to probe couplings $\sim few \times 0.01$, provided sufficient control of the systematics. Interestingly, less constrained models such as the "neutrinophilic scalar" of [11] or the "Dirac neutrino portal" [68] fall in category (A). For the neutrinophilic scalar, we expect the m_W measurement to be the best

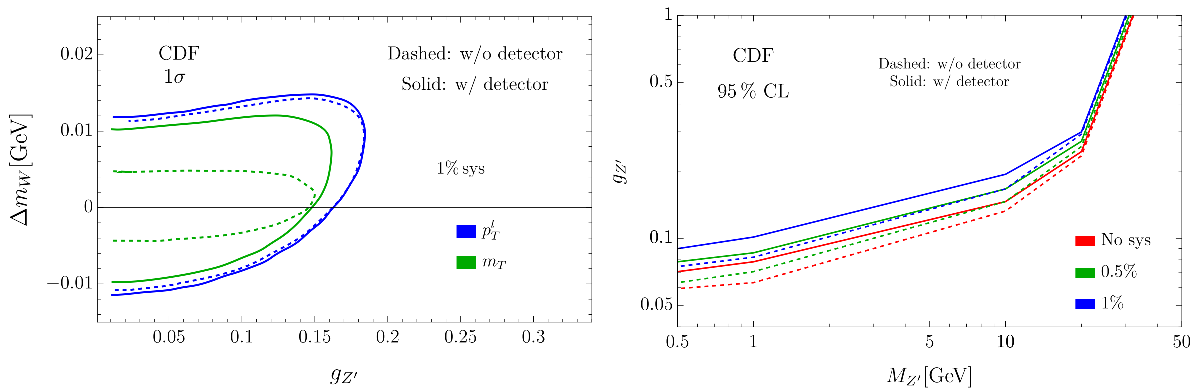

(a) CDF 2D fit

(b) CDF projected sensitivity

Figure 4.4: (a) 2D fit with 68% CL projected sensitivity to $L_\mu - L_\tau$ for $m_{Z'} = 10$ GeV and (b) 95% CL projected sensitivity to $L_\mu - L_\tau$ combining p_T^ℓ, $p_T^{\rm miss}$, and m_T at CDF. The solid lines and dashed lines represent the results when detector effects are included and when they are not included, respectively.

probe [69].

4.2.1.1 The $L_\mu - L_\tau$ gauge boson at CDF

We describe the CDF analysis for the $L_\mu - L_\tau$ Z'-boson model [37]. The cuts are slightly modified from those imposed by CDF for the measurement of m_W, shown in table 4.1. The SM and the NP events, without detector effects, are simulated using MADGRAPH5_AMC@NLOV3.42 [59] + PYTHIA8.212 [60]. We simulate detector effects such as smearing of lepton momentum and hadronic recoil, including pileup, following Ref. [4], such that the distributions resemble those published by CDF.

The simultaneous fit of Δ_{m_W} and $g_{Z'}$ is then performed for m_T, p_T^ℓ and $p_T^{\rm miss}$ distributions. The 1σ contours for m_T and p_T^ℓ are reported in Fig. 4.4a for $m_{Z'} = 10$ GeV. The correlation between $g_{Z'}$ and the measured m_W for both m_T and p_T contours in the presence of detector effects. When detector effects are not present, this correlation is absent for m_T. This suggests that the detector effects are responsible for larger $g_{Z'}$ preferring positive Δ_{m_W} for the fit using

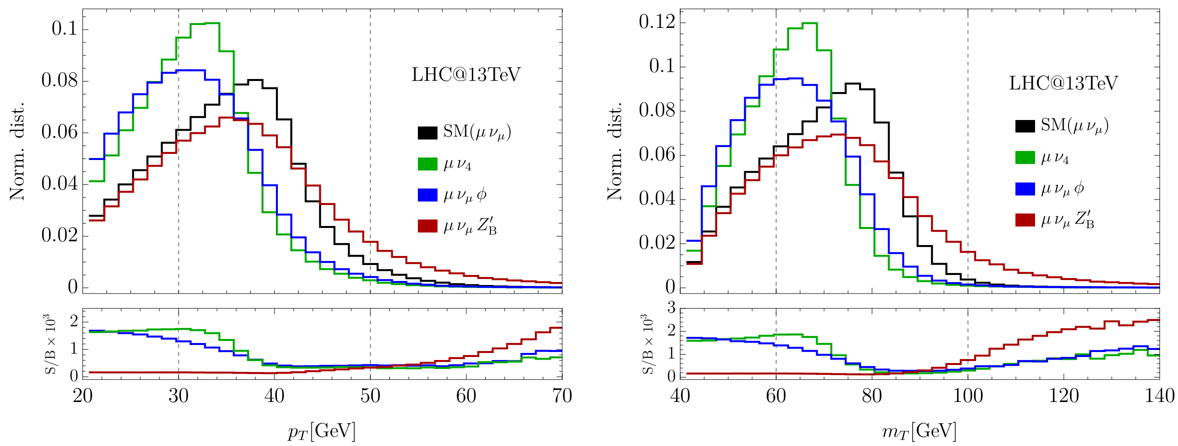

(a) Lepton transverse momentum distributions (b) Transverse mass distributions

Figure 4.5: Distributions of kinematic observables p_T^ℓ and m_T for modified W boson decay and the SM W decay in black. The dashed lines indicate the regions used to extract m_W by ATLAS [3].

m_T. This correlation is small compared to that of ATLAS (in Fig. 3 of the main text) because the pileup effects are much smaller at CDF. This holds true for p_T^ℓ as well since the Jacobian peak is sharper at CDF. These observations may change with a different treatment of the pileup in our simulation.

Next, for CDF, projected sensitivity to the NP parameters are obtained by marginalizing over Δ_{m_W}. The χ^2 from p_T^ℓ, m_t, and p_T^{miss} are combined (without correlation) to obtain exclusion contours. Fig. 4.4b shows a sensitivity which is comparable to the ATLAS projections for this model. Since the NP signal populates the SM-dominated region, the reach at ATLAS is limited by systematics. Hence, even with lower statistics, CDF is competitive. However, CDF's sensitivity is unable to improve since no more data is being collected to lower the statistical uncertainties.

4.2.2 Neutrinophilic scalar ϕ

Next we consider the sensitivity of m_W to a neutrinophilic scalar ϕ, whose model details are described in Section 3.1.2.

We show in Fig. 4.5 the p_T^ℓ and m_T distributions of this anomalous decay (blue lines), compared to the SM (black lines) for a benchmark point in the new physics parameter space. As expected, the net effect is that both distributions become softer, populating the region below the Jacobian peak from on-shell W production. The softening of these spectra is expected, as it is unavoidable that a certain fraction of the W energy is taken away by ϕ. For this analysis, we thus focus on the sub-electroweak strategy, mostly following the ATLAS [2, 3] and CDF [4] analyses. We depart from the exact selection of ATLAS and CDF in that we slightly enlarge the analysis ranges of each observable (see Table 4.1 for details). The use of slightly larger analysis ranges is not crucial to bound new physics with our method, but there is a clear improvement from using the proposed analysis ranges in our analysis described in Sec. 4.1. We remark that in this analysis, we use the same cut on recoil u_T, thus leaving the QCD aspects of the analysis substantially unchanged. Most of the gain comes from including softer m_T and p_T^ℓ, which appears safe from the systematics point of view. In any case, the final assessment of the optimal range for this search needs to be determined by the experiments themselves.

Before describing the sensitivity projections from the sub-electroweak strategy to this model, we first investigate the impact of this scenario on the determination of m_W. We focus on the $\mu + \not{E}_T$ final state. In principle, the electron final state can be equally sensitive, but we do not pursue it as it involves different detector effects. We fix the value of the new scalar mass to $M_\phi = 10$ GeV and study the $\chi^2_{\mathcal{O}}$ in Eq. (4.1) in the $(|\lambda_{\mu\mu}|, \Delta m_W)$ plane. The result is reported in

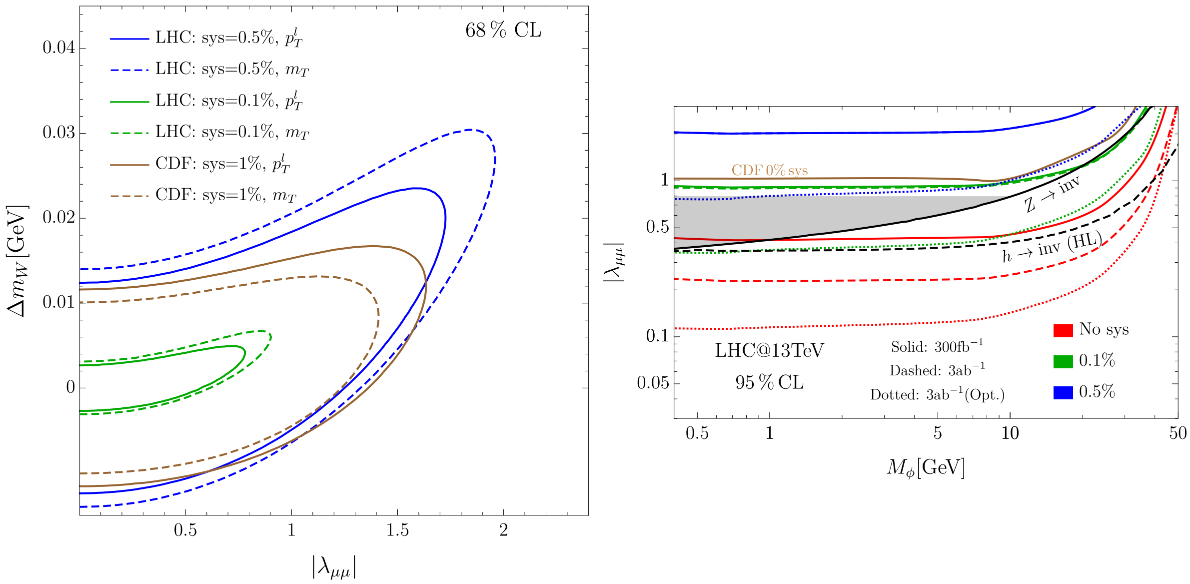

Figure 4.6: Sensitivity projections for the neutrinophilic scalar model. Left panel: 68% CL reach on the $(|\lambda_{\mu\mu}|, \Delta m_W)$ plane with $M_\phi = 10$ GeV. Right panel: 95% CL reach on the $(M_\phi, |\lambda_{\mu\mu}|)$ plane. Current constraints from invisible Z decays and projected constraints from invisible Higgs decays are taken from [11]. In the constraint from invisible Z decays, the gray band gives a rough measure of the uncertainty related to higher order corrections. For the solid and dashed lines of our projections we adopt the benchmark setup described in Section 4.1 and we marginalize on m_W. The dotted lines assume an "optimistic" setup and set $\Delta m_W = 0$. See main text for details.

the left panel of Fig. 4.6 for m_T and p_T^ℓ, LHC and Tevatron colliders, and several possible choices of systematics. For this analysis, we adopt the setup and the parameters described in Section 4.1 and Table 4.1. Here we do not report any additional constraints on the new physics parameter space, aiming to show the correlation between m_W and the latter.

Remarkably, there is a nontrivial interplay between the best-fit value for m_W (via Δm_W) and $|\lambda_{\mu\mu}|$. For a non-zero $|\lambda_{\mu\mu}|$, Δm_W slightly prefers a positive value. That can be understood by noticing that three-body decay makes the p_T^ℓ spectrum softer compared to the SM.

Assuming "SM-like" data with a given $\overline{m}_W$, the best fit prefers a shift toward $m_W > \overline{m}_W$ ($\Delta m_W > 0$), as a compromise to partially compensate for the softening of the p_T^ℓ spectrum from the three-body decay. This is completely analogous to what we have found for the invisibly decaying $L_\mu - L_\tau$ scenario in Section 4.2.1. We remark that this effect is present for both p_T^ℓ and m_T, thus seems not to be linked to pile-up and detector responses, which are very different for these two distributions. Comparing results for different degrees of systematics, the effect does not change significantly, as can be observed in Fig. 4.6. A similar effect is observable, but quantitatively milder, for the CDF. A main difference between the CDF and ATLAS selections is related to the fact that CDF requires smaller hadronic activity (see Table 4.1). This results in sharper kinematic distributions[3] on which it is harder to hide the soft lepton contribution for the three-body decay of this model.

In the right panel of Fig. 4.6, we give the sensitivity projections on the $(M_\phi, |\lambda_{\mu\mu}|)$ plane. The 95% CL value for $|\lambda_{\mu\mu}|$ is obtained for each M_ϕ from a combined χ^2 summing independent χ^2 values of the form Eq. (4.1) for each distribution. For LHC, we minimize $\chi^2 = \chi^2_{m_T} + \chi^2_{p_T^\ell}$, and for CDF we minimize $\chi^2 = \chi^2_{m_T} + \chi^2_{p_T^\ell} + \chi^2_{p_T^{\text{miss}}}$. In the same plane, we also report the main constraints from other searches. In particular, masses below $M_\phi \lesssim 0.5$ GeV are heavily constrained by meson decay spectra [11]. We omit this bound by only showing the parameter space for $M_\phi > 0.5$ GeV. Larger masses are well tested by the precise measurement of the Z-boson invisible decay width and will be better tested by invisible Higgs decays. The latter will be mostly effective at the High Luminosity stage of the LHC. Additional constraints on the region of interest are expected from DUNE and by a direct test of the interaction in Eq. (3.3) (see [11] for a comprehensive list of constraints). These cover only a few corners of the parameter space in Fig. 4.6, hence we omit them for the sake of clarity of the figure. Regarding the bound from Z-boson decays to invisible extracted from [11], in Fig. 4.6 we report a band rather than

[3]In the limit that the hadronic recoil $\vec{u}_T \to 0$, W bosons are produced at rest, and the resulting kinematic distributions p_T^ℓ and m_T have a sharp Jacobian peak with a steep edge.

a line. The reason is that in [11] no loop corrections to $Z \to \nu\nu$ decays, induced by loops of ϕ, are considered. Consequently, the Z decay to invisible gets an unphysical divergence for low masses M_ϕ of the form $\log \frac{m_Z}{M_\phi}$ [40] and this strengthens the corresponding bound. Thus, we obtain the band in Fig. 4.6 from the line of [11] and assuming the corresponding bound to become insensitive to M_ϕ below 10 GeV. We believe that this provides a conservative, yet realistic, estimate. The most up-to-date bound on invisible Z decays is provided in [70], where the cancellation effect was confirmed with explicit 1-loop calculations and intereference with the tree-level SM decay.

In Fig. 4.6, we report 9 different lines corresponding to the expected bounds from the proposed analysis for variations of systematics, statistical treatment, and assumed luminosity. Specifically, for all the solid and dashed lines, we follow the benchmark setup described in Section 4.1 and Table 4.1 with various luminosities and systematics indicated in the figure. Furthermore, aiming at a conservative result, we obtain these lines marginalizing over Δm_W. We also follow the same procedure for the CDF projections. The dotted lines show "optimistic" projections for our methods applied at the HL-LHC. These projections are valid for different degrees of systematic uncertainties, negligible effect of pile-up, finer bin size of 0.25 GeV for p_T^ℓ and 0.5 GeV for m_T, and, finally, assuming prior knowledge of m_W, i.e., fixing $\Delta m_W = 0$.

All in all, Fig. 4.6 suggests that the same data currently employed for the W boson mass measurement can be repurposed to provide a competitive probe of this model. As in many cases with precision physics analyses, this method can yield very remarkable results, complementing and even superseding the other proposed probes of the neutrinophilic scalar if one keeps the systematic uncertainties under good control.

4.2.3 Two-body decay into a heavy neutrino ν_4

Finally in the modified decay category, we consider the sensitivity of m_W to the heavy neutrino model, described in Section 3.1.3. As done with earlier models, the resulting m_T and p_T^ℓ distributions are shown in Fig. 4.5 (green lines). Both spectra get softer than what is expected in the SM, as it is expected on general ground for models that affect the decay of real W bosons. We therefore slightly extend the analysis ranges compared to the ATLAS and CDF measurements, as to include softer p_T^ℓ and m_T. In Table 4.1 we give the exact ranges that we find to maximize the sensitivity to this model from the analysis described in Section 4.1. As in the case of the neutrinophilic scalar, the use of slightly larger analysis ranges is not crucial to bound new physics with our method, but again a clear improvement is expected by using the proposed analysis ranges. As we have commented already, systematic uncertainties play a great role in our strategy thus a final assessment of the optimal range for this search needs to be determined by the experimental collaborations.

In Fig. 4.7 we present our results for this scenario. We focus on the $\mu + \not{E}_T$ final state. In principle, the electron final state can be equally sensitive, but we do not pursue it as it involves different detector effects. The impact of this model on the determination of m_W on the $(|U_{4\mu}|^2, \Delta m_W)$ plane is presented in the left panel of Fig. 4.7. The figure is obtained taking the baseline setup described in Section 4.1 and setting $m_{\nu_4} = 10$ GeV and studying each $\chi^2_{\mathcal{O}}$ as indicated by the labels in the figure. Interestingly, a nontrivial correlation between the mixing $U_{4\mu}$ and Δm_W exists in both CDF and LHC projections, which shows again how new physics can effectively bias the extraction of m_W. Yet, we see that the overall effect in this scenario is quite mild, considering the values of $U_{4\mu}$ for which we find a sizeable Δm_W shift are well tested by

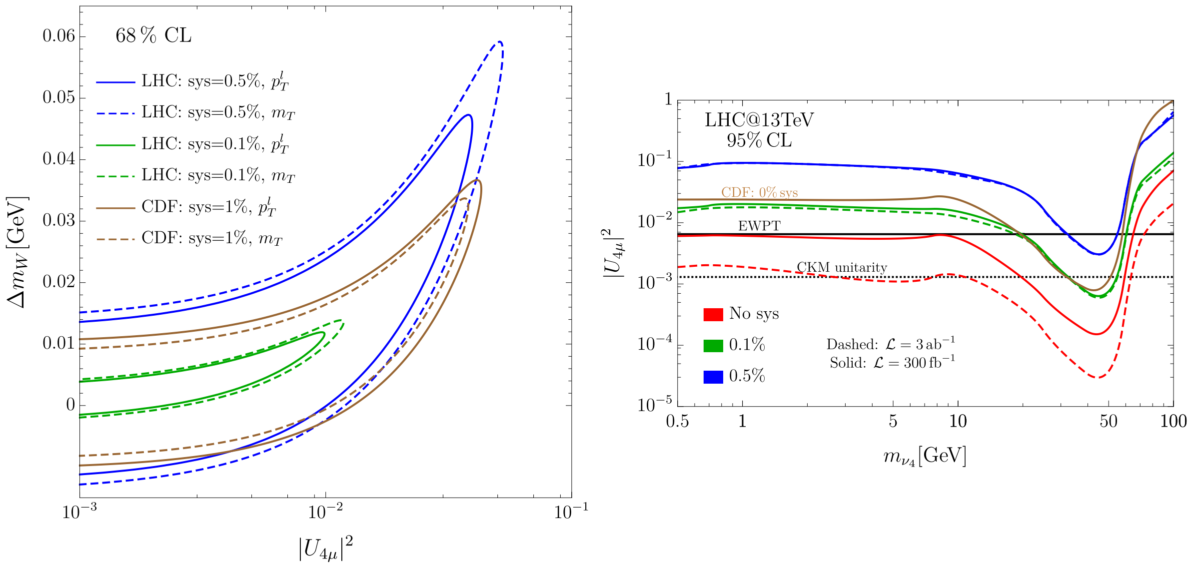

Figure 4.7: Sensitivity projections for the heavy neutrino scenario. Left panel: 68% CL reach on the $(|U_{4\mu}|^2, \Delta m_W)$ plane for $m_{\nu_4} = 10$ GeV. Right panel: 95% CL reach on the $(m_{\nu_4}, |U_{4\mu}|^2)$ plane. Present constraints are extracted from [12]. Our constraints are expected to be roughly the same for electrons (U_{4e}), where the CKM unitarity bound does not apply.

other experiments, for which we refer to the right panel of Fig. 4.7.

Sensitivity projections for our method and other experiments, taken from [12], are presented on the $(m_{\nu_4}, |U_{4\mu}|^2)$ plane in the right panel of Fig. 4.7. We stress that for this analysis we employ the baseline setup of Section 4.1 and give bounds on $U_{4\mu}$ marginalizing on Δm_W. This gives conservative bounds on this new physics mixing parameter. Our bounds complement nicely the existing ones. Specifically, in the sub-GeV region, the most stringent constraints come from high-intensity meson decay studies. We do not show this bound since Fig. 4.7 considers $m_{\nu_4} > 0.5$ GeV. In the region from few GeV to m_W, main constraints are either from electroweak precision tests or from the test of the CKM unitarity [12] in the same ballpark as the projected constraints from our method. For heavier ν_4 our bounds are particularly effective as the change in the shape of the kinematic distributions is most evident. We remark that CKM unitarity bounds apply only to the muonic final state, as they come from meson decays, which produce mostly muon flavor. Bounds from our method can be applied equally well to electrons and muons. Therefore, we expect that the constraints from the measured spectrum of the m_W distribution can be particularly competitive for ν_4 coupled mostly to electrons.

4.3 Probing Modified W Production in the Sub-EW Region

As anticipated, the resulting kinematic distributions give harder spectra than those in the SM, which are shown in Fig. 4.5 for p_T^ℓ and m_T. This motivates us to slightly extend the analysis ranges toward higher p_T^ℓ and m_T compared to the existing ATLAS measurements (see Table 4.1) in the sub-electroweak region. This model could also be studied in the circa-electroweak region, but for this work, we only focus on the sub-electroweak strategy aimed at showing the interplay between the W-mass measurement and relatively light new physics. In the high-end part of these extended ranges, the SM production gets less and less copious for larger and larger values of p_T^ℓ and m_T. This makes the sensitivity of CDF drop significantly compared to previous new physics models. Therefore, we do not include CDF in this analysis.

To determine the sensitivity of the observables used in the W mass measurements, we study the $\chi^2 = \chi^2_{m_T} + \chi^2_{p_T^\ell}$ computed as described in Section 4.1. At variance with the models studied above, we explicitly simulate only the final state $\mu + \not{E}_T$ and take into account electrons as a doubling of the rates in each bin. This gives a fair estimate of the sensitivity of our method in the case in which systematics are negligible. This is quite accurate as most of the sensitivity in this model comes from the extended analysis ranges described above.

Unlike in the previous models, the emission of Z_B' can affect other processes, including the production of Z bosons, which is used as calibration for the MC used to obtain data-driven predictions, and especially for the reduction of systematic uncertainties in [2]. The $Z_B^{\prime}$ can in principle impact the calibration of MC prediction, and can thus remove part or all the sensitivity of the $\ell + \not{E}_T$ channel. Such an effect can be mitigated by imposing a $\not{E}_T$ cut in the selection of the events used for the calibrating from the process $pp \to Z \to \ell\ell$ that can effectively remove $pp \to ZZ_B^{\prime}$. In the following, we do not provide a detailed discussion about this effect, as it is beyond the scope of our work. Rather, we only emphasize that such an effect should be assessed appropriately by the experimental collaborations when implementing the analysis for this model.

Under the provisions explained above we show the projected sensitivity to the hadrophilic $Z_B^{\prime}$ in Fig. 4.8. The impact of this model on the m_W measurement is reported in the $(g_{Z_B^{\prime}}, \Delta m_W)$ plane, for a fixed value $M_{Z_B^{\prime}} = 10$ GeV. Interestingly, also in this model there is some correlation between the preferred value for Δm_W and $g_{Z_B^{\prime}}$. In contrast to the previously discussed scenarios with modified decays (see Figs. 4.6 and 4.7), the preferred mass difference Δm_W is negative. The possible effect on the m_W value appears to be limited to *few* MeV.

The sensitivity projections on the $(M_{Z_B^{\prime}}, g_{Z_B^{\prime}})$ plane are presented in the right panel of Fig. 4.8 together with constraints on this scenario from other searches. The main constraints arise from the Run-2 mono-photon and mono-jet searches at the LHC [6,13,71] with an integrated luminosity 138 fb^{-1}. These searches report their results in the context of a simplified model in which a new gauge boson $A^{\prime}$ (dubbed "mediator") couples to dark matter χ and to the quarks. We must adapt the bounds provided in this model to fit our needs. In particular, there are no public results for a new gauge boson lighter than 50 GeV decaying into dark matter.[4] Therefore, we recast the results of these analyses to estimate a bound on the coupling $g_{Z_B^{\prime}}$ in the region of

[4] We stress that the absence of these light new physics spectra in the publicly available limits is a delicate point. As a matter of fact, we find that these spectra have significantly relaxed bounds on the new physics coupling, thus potentially indicating a loophole of the standard searches.

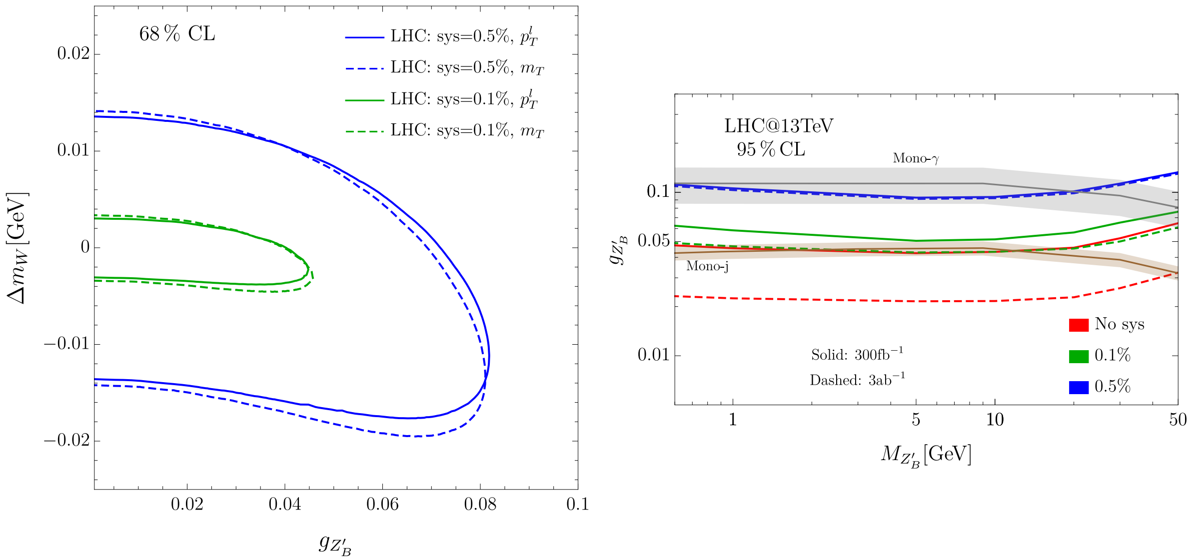

Figure 4.8: Sensitivity projections for the hadrophilic Z' scenario. Left panel: 68% CL reach on the $(g_{Z'_B}, \Delta m_W)$ plane with $M_{Z'_B}$ set to be 10 GeV. Right panel: 95% CL reach on the $(M_{Z'_B}, g_{Z'_B})$ plane. Existing constraints from mono-jet and mono-photon are obtained by recasts of [6,13] (see the text for more details).

interest for our work $M_{Z'_B} \in [0.5, 50]$ GeV, assuming $M_\chi = M_{Z'_B}/3$. For lighter Z'_B we expect our recast to not be sensitive to the exact mass $M_{Z'_B}$. Lighter M_χ would also not significantly change our recast, as the kinematics of the decay $Z'_B \to \chi\chi$ is controlled by $\beta^2 = M^2_{Z'_B}/(4M^2_\chi)$.

For our recast, we simulate at LO the process $pp \to A' + X$ for $X = jet, \gamma$ with MadGraph5_aMC@NLO v3.42 [59] using a UFO [72] implementation of the model DMsimp_s_spin1 used by the experiments [73, 74]. We pick as recast bound the strongest bound obtained among the several inclusive signal regions considered by the relevant experimental works [6, 13, 71]. We checked the accuracy of this method for choices of $M_{A'}$ and M_χ as close as possible to our case and we find that we reproduce the results of the mono-photon search up to a factor 25% in the coupling $g_{Z'_B}$. For the mono-jet recast, we need to adjust our result, strengthening the constraint by a factor of 2. We observe that these adjustment factors are quite close to a constant for mono-jet, within 10% in our set of spectra, and have a stronger variability than for mono-photon. Thus, we consider our mono-jet recast to have a 10% uncertainty due to the lack of accuracy of our recast. For the mono-photon bound, we do not need to adjust the results, and we conservatively ascribe a 25% uncertainty. The origin of these mismatches is not investigated further, as we intend to only obtain a ballpark value for the bound that the experimental collaboration might put on this scenario if they use traditional mono-X searches.

The bound from the recasting of the mono-jet and mono-photon searches and the bounds that we find with our method are shown in the right panel of Fig. 4.8. All in all, we find that the recast mono-jet bounds are comparable with those from the precision study of the $\ell + \not{E}_T$ final state. We remark that for our method we present bounds on the new physics coupling marginalizing on Δm_W in our χ^2, which results in conservative bounds on new physics.

It is worth noting that, even for small systematic uncertainties around 0.1%, improvements are to be expected going from the LHC to the HL-LHC. This behavior is not observed in the previous analyses in Section 4.2, where the reach is dominated by systematics already at the LHC. This difference can be ascribed to the fact that new physics in the decay of the W boson affects the soft part of the distribution, where the highest-rate backgrounds populate the phase-space. On the contrary, in the case of production of W associated with new physics, the effects on the kinematic distributions extend to the regions of phases-space that are not so copiously populated by SM processes, on which the higher statistics of the HL-LHC is expected to bring the most benefits.

4.4 Probing $\ell + \not{E}_T$ without on-shell W in the Sub-EW Region

We now turn to the minimal supersymmetric standard model (MSSM) [55], which offers a simple irreducible "background" for the m_W measurement: "left-handed" $SU(2)_L$ doublet slepton-sneutrino production, with subsequent decay into lepton plus only invisible particles (see Fig. 3.5),

$$pp \to \tilde{\ell}(\to \ell\, \tilde{\chi}_1^0)\, \tilde{\nu}_\ell\,. \tag{4.4}$$

In this scenario, both the sneutrino and neutralino are invisible, and either one could be the lightest stable particle (LSP).[5] More details For simplicity, we assume that the other superpartners, including $SU(2)_L$ singlet – or right-handed sleptons – are heavy, thus having negligible cross-sections at the LHC.

Sleptons lighter than 100 GeV are excluded by LEP [75–79]. Sleptons heavier than the LEP bound have negligible cross-section at the Tevatron so we do not consider CDF in this section. LHC searches for di-sleptons [14, 80] are sensitive to sleptons above the LEP bounds but suffer when the sleptons and $\tilde{\chi}^0$ are close by in mass. In particular, when the mass gap $m_{\tilde{\ell}} - m_{\tilde{\chi}_0} \sim m_W$, the lepton p_T resembles that of the lepton from SM W-boson decay. This compressed region of parameter space is dominated by SM events and requires a dedicated analysis. In [81, 82] it has been proposed to use precision measurements to disentangle WW events from di-slepton production. Yet, there is still some uncovered gap in the parameter space in the experimental results (see our summary of present constraints in Fig. 4.9). Addressing this shortcoming of the

[5] When the lightest neutralino $\tilde{\chi}_1^0$ is the LSP, $\tilde{\ell} \to \ell\, \tilde{\chi}_1^0$, and $\tilde{\nu} \to \nu\, \tilde{\chi}_1^0$, as illustrated in Fig. 3.5, produces the $\ell + \not{E}_T$ final state. If the sneutrino is the LSP (not shown), then $\tilde{\chi}_1^0 \to \tilde{\nu}\, \nu$ also maintains the $\ell + \not{E}_T$ final state.

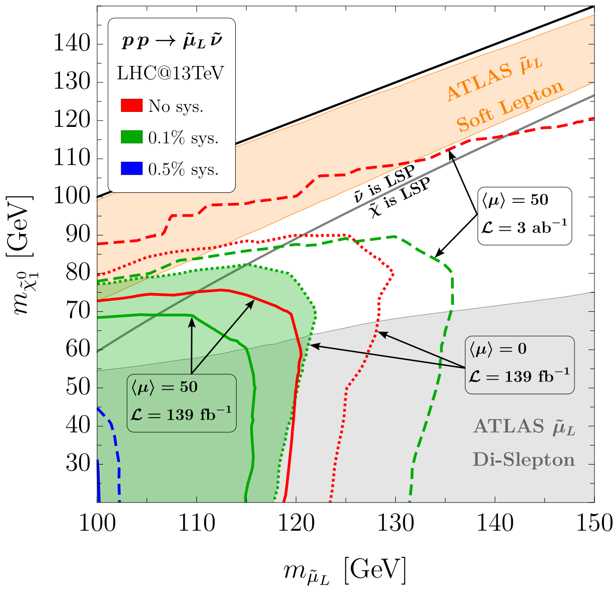

Figure 4.9: LHC 95% CL projected sensitivity to MSSM slepton-sneutrino production from our proposal. All of our projections include detector simulations. Pileup ($\langle\mu\rangle = 50$), simulated through the dedicated DELPHES ATLAS card, is included unless indicated otherwise. Present bounds (gray and orange shaded areas) from the ATLAS experiment are adapted from Ref. [14]. Our results are the **green shaded area**, for the present $\mathcal{L} = 139\,\text{fb}^{-1}$ integrated luminosity and 0.1% systematics. We also present results under several different pile-up and integrated luminosity options in colors and dashed or dotted lines, as indicated in the plot.

present searches by filling this gap is a main result of this letter.

The phenomenology of the process in Eq. (4.4) belongs to category (C), since no on-shell W-boson is produced (see Fig. 3.5). As shown in Fig. 4.5, NP produces a rather flat and extended m_T distribution with a rising S/B ratio at higher m_T, since the process is not initiated by the decay of a resonance. The contamination in the Z-boson sample due to $pp \to \bar{\tilde{\ell}}\tilde{\ell} \to \bar{\ell}\ell\tilde{\chi}_0\tilde{\chi}_0$ is limited to $\mathcal{O}(10^{-5})$.

For this model, we follow the same procedure as described in Section 4.1 of marginalizing on Δ_{m_W} for varying NP parameters. For each point on the $m_{\tilde{\ell}} - m_{\tilde{\chi}_1^0}$ plane, m_W is varied as an input in the template, and the minimum χ^2 is obtained from the fit. The m_W determination is largely governed by the peak positions of p_T^ℓ and m_T spectra. Therefore, the rather flat kinematic distributions of NP contributions make a milder impact on the m_W measurement than what is shown in, for example, Fig. 4.2b. Sensitivity projections are reported in Fig. 4.9 as functions of $(m_{\tilde{\ell}}, m_{\tilde{\chi}_0})$. The sneutrino mass is fixed at the lowest allowed value in the MSSM, assuming the large $\tan\beta$ limit [55].

Two sets of expected sensitivities are reported in Fig. 4.9, corresponding to the inclusion or not of pileup. In both cases, the fitting range (see Table 4.1) is chosen to cover part of the unexplored parameter space. Extending the range to higher m_T, still keeping sufficient control of the systematics, might improve the sensitivity, as shown in Fig. 4.5. However, far from the "m_W" region, systematics becomes more challenging. This is caused, for instance, by the limited Z-boson sample available for calibrations, or by the increasing backgrounds. The study of systematics outside of the range presently used for each kinematic distribution employed in the m_W measurement can only be carried out by the experimental collaborations. Here we are pointing out the huge gain in sensitivity to NP that can be obtained by enlarging the fitting range. Ideally ATLAS and CMS experiments will find the best range of each kinematic variable for which the experiment can keep systematics under control so as to maximize the sensitivity to NP.

A significant result of ours is that the same analysis used for the m_W measurement, with only a slightly extended fitting range, can put new bounds and potentially discover new physics in an unexplored parameter space of MSSM. Additionally, the increasing S/B ratio for MSSM slepton-sneutrino production motivates a search at higher p_T^{ℓ} and m_T, which is the circa-EW strategy shown in the following chapter.

Chapter 5: Circa-Electroweak Analysis

We now shift away from the Jacobian peak of the SM W, considering a different region of p_T^ℓ and m_T. Now the background is dominantly offshell Drell-Yan production of $\ell + \not{E}_T$, which has very little dependence on the precise value of m_W. Hence, this analysis does not require a simultaneous fitting of SM and NP parameters. However, this search strategy is not identical to the usual search strategy in the high energy (supra-EW) regime $>$ TeV. This strategy is a more targeted search for NP whose kinematic distributions lie between the sub-EW region where m_W is measured and the supra-EW region.

As discussed in detail later in Section 5.1, some sensitivity to BSM comes from the p_T range beyond the SM Jacobian peak [5]. Therefore, we consider the possibility to perform the search for BSM physics in a different range than what considered in the measurement of m_W. We focus in particular on new physics appearing at a mass scale around the weak scale, and thus, we denote the associated region and strategy as "circa-electroweak."

We will again use the example of sleptons in the MSSM right above the LEP limits to display one instance of this kind of search. In this context, we will illustrate how the proposed search strategy can fill gaps of current searches. This analysis does not overlap with the sub-electroweak analysis, and can therefore be considered an independent study.

The analysis has some slight differences compared to the sub-EW analysis. First of all, it differs for the range of kinematic quantities that we use in our likelihood computations from SM templates and pseudo-data from BSM signals. For illustration of the selection we will use, we refer the reader to Table 5.1. Furthermore, in this analysis, part of the sensitivity stems from the overall number of events. Thus, unlike for the sub-electroweak analysis, we do not normalize the predicted SM distributions to the pseudo-data. For this reason, we include a correlated error $\epsilon^{\rm cor} = 2\%$, a conservative estimate based on LHC Run-2 analyses [14, 80]. We consider a few benchmark points for the uncorrelated per-bin systematics: $\epsilon^{\rm unc} = 0\%,\ 2\%,\ 5\%$, and 10% for the LHC projections. Unlike for the sub-electroweak analysis, the CDF projections are not included, as the final-state particles are heavy enough ($m_{\tilde{\ell}} \gtrsim 100$ GeV) to render the cross-sections at CDF negligible. Finally, a very important point is that in the circa-electroweak analysis, the exact value of the W-boson mass is not a crucial input. This is because the majority of the sensitivity to new physics comes from regions of the kinematic distributions in which the SM processes are relatively rare, thus a moderately large S/B is typical for this search strategy. Thus, after careful testing of this step, we assume m_W to be a known parameter from other experiments or other analyses, or both, and set $\Delta m_W = 0$ in Eq. (4.1).

5.1 MSSM Slepton-Sneutrino Production in the Circa-EW Region

This analysis completes and extends our previous results in Section 4.4. More precisely, in the previous chapter,we focused on the sub-electroweak strategy, showing that the same data responsible for the W boson mass measurement are particularly sensitive to the MSSM compressed region $m_{\tilde{\mu}} - m_{\tilde{\chi}} \lesssim m_W$ via $\tilde{\ell}\,\tilde{\nu}_\ell$. In the present work, we reconsider this channel to assess the sensitivity of data at higher-p_T considering the *circa*-electroweak strategy as well. The main

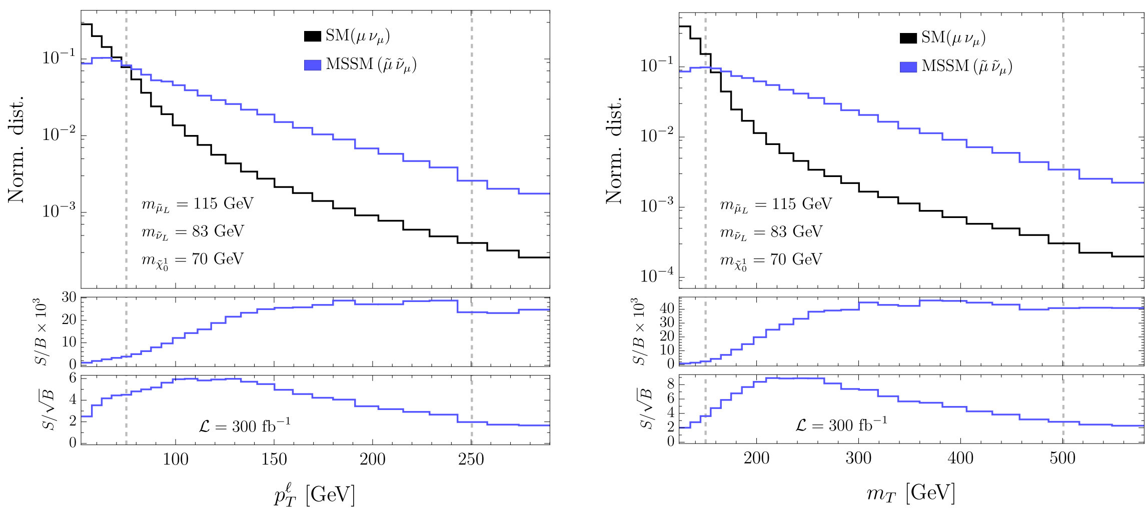

Figure 5.1: Distributions of SUSY slepton-sneutrino production as signal and Drell-Yan as background for p_T^ℓ on the left and m_T on the right. The bottom panels show S/B and S/$\sqrt{B}$ for $\mathcal{L} = 300$ fb^{-1}. The selections for both panels are inspired by the CMS W' search and are summarized in Tab. 5.1. The binning is described in the text. The vertical dashed lines delimit the range we use for our analysis. The SUSY distributions are taken from a benchmark point of ($m_{\tilde{\mu}_L}$ = 115 GeV, $m_{\tilde{\nu}_L}$ = 83 GeV, $m_{\tilde{\chi}_0^1}$ = 70 GeV). The kinematic ranges shown here correspond to the circa-electroweak region shown in Fig. 1.2.

reason for bringing our attention to this region is that more canonical analyses, e.g., standard W' searches [23], have focused mostly on very large p_T values, ending up pursuing new physics in the $supra$-electroweak regime.

As it can be inferred from the S/B ratio shown in Fig. 5.1, valuable sensitivity to new physics arises at moderate p_T not far from the typical values used in the analysis devoted to high-precision m_W measurements. To pursue such new physics we adopt the selection reported in Tab. 5.1. For comparison, we also report in the table the selection used by W' searches of CMS. We stress that the selection criteria are largely borrowed from the W' search and not optimized to isolate slepton-sneutrino production. However, the survival rate of the SUSY signals is large enough to give us sensitivity to explore the compressed region of the parameter space that is currently beyond the reach of conventional dislepton searches [14, 80, 83].

	W' (μ) [23]	MSSM
p_T^ℓ minimum (GeV)	> 50	> 50
$p_T^\ell / p_T^{\text{miss}}$	> 0.4 & < 1.5	> 0.4 & < 1.5
m_T minimum (GeV)	> 120	> 120
$\Delta\phi(\vec{p}_T^{\,\ell}, \vec{p}_T^{\,\text{miss}})$	> 2.5	> 2.5
p_T^ℓ range (GeV)	$[50, 4000]$	$[75, 250]$
m_T range (GeV)	$[120, 7000]$	$[150, 500]$
p_T^ℓ bin width (GeV)	80	$5 - 14$
m_T bin width (GeV)	98	$10 - 28$

Table 5.1: Kinematic cuts, analysis ranges, and bin widths considered for our MSSM slepton-sneutrino analysis, compared to those used in the W' search by CMS.

The main difference of our strategy from the W' search is that we pursue a more refined analysis of the shape of the kinematic distributions with finer bins. For reference, we recall that near the Jacobian peak of the p_T^ℓ distribution, a bin width of 1 GeV is used by CDF and ATLAS. Beyond the Jacobian peak the SM rate decreases, thus larger bins are desirable to keep the statistical uncertainty low enough. For our analysis, we find a good balance using 5 GeV bin width for $p_T^\ell \in [75, 90]$ GeV and exponentially growing bins[1] for $90 < p_T^\ell < 250$ GeV. For m_T, the bin widths are twice those of p_T^ℓ, as the associated analysis range is doubled from that of p_T^ℓ. The resulting distributions of p_T^ℓ and m_T for MSSM sleptons and SM background $pp \to \mu\nu$ are shown in Fig. 5.1.

The data at large p_T is not used in our analysis, as the mass scale of the new physics that we are after implies no new physics effects to be expected there. Indeed, we cap the analysis ranges for our analysis by looking at the $S/\sqrt{B}$ and S/B distributions for the signal of interest, aiming to include the peak of the $S/\sqrt{B}$ and some padding around it, see for example, Fig. 5.1. We remark that our results depend only mildly on the exact location of the end-point of the analysis

[1]The exact formula to obtain the edges of the p_T^ℓ bins is the following: bin edges are given by $b = e^x$, where x ranges from $\ln(p_T^{\text{min}}/\text{GeV})$ to $\ln(p_T^{\text{max}}/\text{GeV})$, with $\Delta x = [\ln(p_T^{\text{max}}/\text{GeV}) - \ln(p_T^{\text{min}}/\text{GeV})]/n$, where $n = 20$ is the number of bins. This gives $n+1$ bin edges, corresponding to n bins.

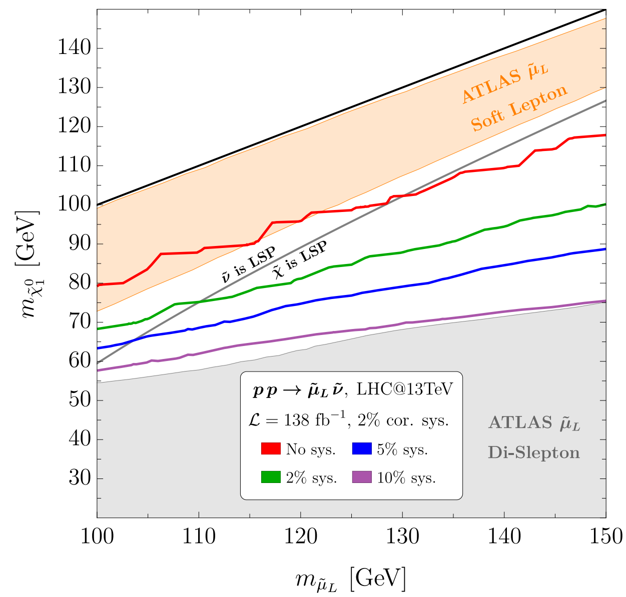

Figure 5.2: The 95% CL projected sensitivity to SUSY slepton-sneutrino production at LHC, using p_T^ℓ and m_T distributions beyond the Jacobian peak of the SM W boson DY production. The analysis is summarized in Table 5.1.

range around the values indicated in Tab. 5.1.

In our projections, we only consider Drell-Yan (DY) W boson production as background, and we do not include other possible sources of SM backgrounds such as single top production, top quark pair production $t\bar{t}$, diboson production WW and WZ, τ, and mistagged Z. After imposing our cuts, we find that these subdominant backgrounds only contribute less than 4% of DY and therefore are ignored for the rest of the analysis.

In the spirit of complementing our work shown in Section 4.4, which was focused on the repurposing the m_W measurement via sub-EW analyses, in this work we consider an analysis range that does not include the Jacobian peak of SM W boson production. For this reason, we expect that the sensitivity of this analysis to variations of the measured mass of the W boson is negligible. Therefore, when obtaining the χ^2 for a choice of SUSY parameters, m_W is not a marginalized parameter. Instead, m_W is fixed to the measured ATLAS value throughout. The

χ^2 that we study is $\chi^2_{p_T} + \chi^2_{m_T}$. We compute its values comparing the LO theory SM prediction, assumed to be the measured data, with templates in which we vary the slepton and neutralino masses $m_{\tilde{\ell}}$ and $m_{\tilde{\chi}^0_1}$. The sneutrino mass is a dependent parameter, that we obtain from the slepton mass saturating the D-term relation in the MSSM [55, 58].

In Fig. 5.2, we show 95% CL sensitivity projections for the LHC current luminosity 139 fb^{-1}, assuming a 2% correlated systematics on the luminosity, and additional uncorrelated per-bin systematics as per the color code ranging from 0 to 10%. It is worth noting that the benchmark uncorrelated systematics that we employed are quite smaller compared to the W' search [23]. Our choice seems tenable, however, because we focus our analysis on the region between $200 - 400$ GeV, whereas [23] insists on much larger values of p_T and m_T on the TeV tail of the kinematic distributions. In the figure, we also show the part of the plane currently probe by ATLAS searches for MSSM production of smuons. Notably, the method that we propose is sensitive to regions of the slepton-neutralino mass plane not covered by present searches.

Finally, we remark that the present analysis is independent of the analysis presented in Section 4.4, as the ranges of p_T and m_T used in the two analyses are disjoint. Thus the present result provides a further complementary new probe to close the gap in the SUSY compressed region, described by our earlier sub-EW analysis in Section 4.4.

Chapter 6: Conclusion

The aim of our work is to assess the sensitivity of high-precision collider data to new physics. We specifically examine the case of $\ell + \not{E}_T$ and focus on new physics signals producing typical lepton p_T softer than the EW scale, $\mathcal{O}(100)$ GeV for which reliable calibration data is available, or slightly harder scale where the SM predictions and detector modeling are still under control. We refer to these two regions as sub-electroweak and circa-electroweak, as illustrated in Fig. 1.2. Unlike the high-p_T region (referred to as supra-electroweak) which has been heavily exploited in conventional new physics searches, the sub- and circa-electroweak regions are not the typical target for BSM. In this paper we demonstrate that, provided sufficient control of the various sources of uncertainties, at a per-mil level in the sub-electroweak or at a percent level in the circa-electroweak, these regions can serve as optimal probes for relatively light new physics, offering complementary tests to other experiments.

Furthermore, BSM searches conducted in regions heavily overlapping with SM measurements exhibit a notable interplay between BSM and SM physics. Specifically, since the same dataset is used for both BSM searches and SM measurements, it necessitates a simultaneous fit of BSM and SM parameters. Consequently, we observe that new physics can bias the extraction of the SM parameters, as we show for the case of the m_W mass measurement, even if only to a limited amount (see Figs. 4.6, 4.7, and 4.8).

We find that it is in the *sub*-electroweak search that the above-mentioned simultaneous fluctuation of SM and NP parameters in the measurements is a key step for unlocking the discovery potential strategy, thus obtaining a measurement combined with limit-setting. The determination of SM parameters is more decoupled from new physics searches in the circa-electroweak strategy. Still, the circa-electroweak strategy benefits hugely from knowing the SM accurately. In fact, the region of phase-space where new physics is expected to appear, though not overlapping with that used for measurements of SM parameters, is influenced by the tails of SM processes. Thus in both cases, there is a nontrivial meshing of SM measurements and searches for new physics.

The list of possible new physics models to which the precision $\ell + \not{E}_T$ can be sensitive is vast. Thus we proceed to identify a few models that can serve as axes of the map of the space of models. The models are chosen for their underlying value as models of new physics as well as for their feature to induce specific modification of the kinematic distributions under study. We present sensitivity projections for (HL-)LHC and CDF to BSM physics belonging to three categories: anomalous W-production (Sections 3.1 and 4.2), anomalous W-decay (Sections 3.2 and 4.3) and new physics producing $\ell + \not{E}_T$ without the propagation of a (nearly) on-shell W (Sections 3.3, 4.4 and 5.1). Each category is illustrated by concrete examples in the corresponding section. The results we have shown in Chapters 4 and 5 cover a large enough set of possibilities that demonstrates the potential to carry out new physics searches in the sub- and circa-electroweak regions by exploiting the highly "curated" data used in precision measurements.

For each scenario, we obtain the following concrete results. We investigate anomalous W boson decays through three examples: the radiative emission of a leptophilic gauge boson (Section 4.2.1), the radiative emission of a neutrinophilic scalar (Section 4.2.2) and the two-body decay of the W into ℓ plus a heavy neutrino (Section 4.2.3). The generic characteristic of these decays is to make the lepton p_T spectrum softer, populating the sub-electroweak region (see Figs. 4.1 and 4.5), the same region responsible for the m_W measurement. In both these examples, we find a nontrivial correlation between the extracted m_W and the new physics parameters as shown in the left panels of Figs. 4.6 and 4.7. Specifically, we find that a positive m_W shift can partially compensate for the effect of new physics and this might result in a smaller extracted m_W in the presence of the latter. This bias turns out to be smaller at CDF than at LHC. This is due to a different selection for the hadronic recoil and, to a smaller extent, to a different impact of pile-up. For the models considered the possible bias is limited to a fraction of the measurement uncertainty from ATLAS. Still these results highlight that more precise measurements in the future may be hindered by bias due to NP and even cause disagreement between LHC and Tevatron results. Regardless of a possible bias in the measurements, we find that the (HL-)LHC can provide a competitive bound for these models, assuming a setup as close as possible to the present W-boson mass measurement (see right panels of Figs. 4.6 and 4.7).

An example of anomalous W production is presented through the initial state radiation of a relatively light ($1 - 50$ GeV) hadrophilic Z' (Section 4.3). In this case the W-boson recoils against the initial state radiation Z', making the p_T spectrum harder. Like the previous example, we find that in the range of interest, the sub-electroweak region can be a sensitive probe for this model. We limit this analysis to the LHC, as CDF statistics is too low to provide a competitive bound. On the one hand, we find that the same dataset employed for the measurement of m_W in the $\ell + \not{E}_T$ final state can provide a probe competitive to present Z' sensitivity from LHC searches in mono-jet or mono-photon. Yet on the other hand, we find again that this kind of BSM can potentially bias m_W with the opposite trend to what is discussed for the anomalous W-decay. Although we have not pursued it in this work, a search in precision data in the circa-electroweak region can be sensitive to this model and could help to disentangle a possible effect on the measurement of m_W.

Finally, we provide a study of new physics populating the sub- and circa-electroweak region via slepton-sneutrino production in the MSSM (Sections 4.4 and 5.1). We show that extending the analysis to the circa-electroweak region provides further sensitivity and improves our sub-EW result, provided control of the systematic uncertainty at a few percent level can be attained in the circa-electroweak region. We remark that this channel was somehow ignored by present LHC searches and has the potential to cover wholly new regions of parameter space of the MSSM (see Figs. 4.9 and 5.2).

With upcoming $\ell + \not{E}_T$ data from the LHC, we foresee opportunities for new physics searches using new observables, such as a doubly differential distribution in lepton p_T and η. This data could potentially be unfolded to the particle level for wider accessibility beyond experimental collaborations, or it could be published together with full information on correlated uncertainties on the kinematic distributions, allowing a more careful re-use and limit-setting from the procedure described above. Furthermore, constraints will strengthen as statistics increase and precision improves at HL-LHC.

We anticipate that as these methods are perfected, testing new physics with a nearly model-independent method becomes possible, enabling the pursuit of elusive models, such as the so-called "inert doublet" [84–86] or other SUSY scenarios [57], which can produce $\ell + \not{E}_T$ but are too faint [87] for present sensitivity.

We believe this strategy to be a novel and promising way to look at present and future collider data, ultimately applicable to a variety of BSM searches and SM measurements.

Bibliography

[1] Gautam Bhattacharyya. A Pedagogical Review of Electroweak Symmetry Breaking Scenarios. *Rept. Prog. Phys.*, 74:026201, 2011.

[2] Morad Aaboud et al. Measurement of the W-boson mass in pp collisions at $\sqrt{s} = 7$ TeV with the ATLAS detector. *Eur. Phys. J. C*, 78(2):110, 2018. [Erratum: Eur.Phys.J.C 78, 898 (2018)].

[3] Improved W boson Mass Measurement using 7 TeV Proton-Proton Collisions with the ATLAS Detector. Technical report, CERN, Geneva, 2023.

[4] T. Aaltonen et al. High-precision measurement of the W boson mass with the CDF II detector. *Science*, 376(6589):170–176, 2022.

[5] J. Smith, W. L. van Neerven, and J. A. M. Vermaseren. The Transverse Mass and Width of the W Boson. *Phys. Rev. Lett.*, 50:1738, 1983.

[6] Armen Tumasyan et al. Search for new particles in events with energetic jets and large missing transverse momentum in proton-proton collisions at $\sqrt{s}$ = 13 TeV. *JHEP*, 11:153, 2021.

[7] Kurt Riesselmann. The standard model of particle physics. *Symmetry Magazine*, 2015.

[8] John Ellis. Higgs Physics. In *2013 European School of High-Energy Physics*, pages 117–168, 2015.

[9] Arno Straessner. Measurement of the W boson mass at LEP. In *39th Rencontres de Moriond on Electroweak Interactions and Unified Theories*, pages 3–10, 5 2004.

[10] Wolfgang Altmannshofer, Stefania Gori, Maxim Pospelov, and Itay Yavin. Neutrino Trident Production: A Powerful Probe of New Physics with Neutrino Beams. *Phys. Rev. Lett.*, 113:091801, 2014.

[11] André de Gouvêa, P.S. Bhupal Dev, Bhaskar Dutta, Tathagata Ghosh, Tao Han, and Yongchao Zhang. Leptonic scalars at the LHC. *Journal of High Energy Physics*, 2020(7), jul 2020.

[12] Brian Batell, Tao Han, David McKeen, and Barmak Shams Es Haghi. Thermal Dark Matter Through the Dirac Neutrino Portal. *Phys. Rev. D*, 97(7):075016, 2018.

[13] Georges Aad et al. Search for dark matter in association with an energetic photon in pp collisions at $\sqrt{s}$ = 13 TeV with the ATLAS detector. *JHEP*, 02:226, 2021.

[14] Georges Aad et al. Search for direct pair production of sleptons and charginos decaying to two leptons and neutralinos with mass splittings near the W-boson mass in $\sqrt{s}$ = 13 TeV pp collisions with the ATLAS detector. *JHEP*, 06:031, 2023.

[15] T. Aoyama, N. Asmussen, M. Benayoun, J. Bijnens, T. Blum, M. Bruno, I. Caprini, C.M. Carloni Calame, M. Cè, G. Colangelo, F. Curciarello, H. Czyż, I. Danilkin, M. Davier, C.T.H. Davies, M. Della Morte, S.I. Eidelman, A.X. El-Khadra, A. Gérardin, D. Giusti, M. Golterman, Steven Gottlieb, V. Gülpers, F. Hagelstein, M. Hayakawa, G. Herdoíza, D.W. Hertzog, A. Hoecker, M. Hoferichter, B.-L. Hoid, R.J. Hudspith, F. Ignatov, T. Izubuchi, F. Jegerlehner, L. Jin, A. Keshavarzi, T. Kinoshita, B. Kubis, A. Kupich, A. Kupść, L. Laub, C. Lehner, L. Lellouch, I. Logashenko, B. Malaescu, K. Maltman, M.K. Marinković, P. Masjuan, A.S. Meyer, H.B. Meyer, T. Mibe, K. Miura, S.E. Müller, M. Nio, D. Nomura, A. Nyffeler, V. Pascalutsa, M. Passera, E. Perez del Rio, S. Peris, A. Portelli, M. Procura, C.F. Redmer, B.L. Roberts, P. Sánchez-Puertas, S. Serednyakov, B. Shwartz, S. Simula, D. Stöckinger, H. Stöckinger-Kim, P. Stoffer, T. Teubner, R. Van de Water, M. Vanderhaeghen, G. Venanzoni, G. von Hippel, H. Wittig, Z. Zhang, M.N. Achasov, A. Bashir, N. Cardoso, B. Chakraborty, E.-H. Chao, J. Charles, A. Crivellin, O. Deineka, A. Denig, C. DeTar, C.A. Dominguez, A.E. Dorokhov, V.P. Druzhinin, G. Eichmann, M. Fael, C.S. Fischer, E. Gámiz, Z. Gelzer, J.R. Green, S. Guellati-Khelifa, D. Hatton, N. Hermansson-Truedsson, S. Holz, B. Hörz, M. Knecht, J. Koponen, A.S. Kronfeld, J. Laiho, S. Leupold, P.B. Mackenzie, W.J. Marciano, C. McNeile, D. Mohler, J. Monnard, E.T. Neil, A.V. Nesterenko, K. Ottnad, V. Pauk, A.E. Radzhabov, E. de Rafael, K. Raya, A. Risch, A. Rodríguez-Sánchez, P. Roig, T. San José, E.P. Solodov, R. Sugar, K. Yu. Todyshev, A. Vainshtein, A. Vaquero Avilés-Casco, E. Weil, J. Wilhelm, R. Williams, and A.S. Zhevlakov. The anomalous magnetic moment of the muon in the standard model. *Physics Reports*, 887:1–166, 2020. The anomalous magnetic moment of the muon in the Standard Model.

[16] B. Abi et al. Measurement of the Positive Muon Anomalous Magnetic Moment to 0.46 ppm. *Phys. Rev. Lett.*, 126(14):141801, 2021.

[17] D. P. Aguillard et al. Measurement of the Positive Muon Anomalous Magnetic Moment to 0.20 ppm. *Phys. Rev. Lett.*, 131(16):161802, 2023.

[18] Sz. Borsanyi et al. Leading hadronic contribution to the muon magnetic moment from lattice QCD. *Nature*, 593(7857):51–55, 2021.

[19] Alessandro Strumia. Interpreting electroweak precision data including the W-mass CDF anomaly. *JHEP*, 08:248, 2022.

[20] Pouya Asadi, Cari Cesarotti, Katherine Fraser, Samuel Homiller, and Aditya Parikh. Oblique Lessons from the W Mass Measurement at CDF II. 4 2022.

[21] Johannes Haller, Andreas Hoecker, Roman Kogler, Klaus Mönig, and Jörg Stelzer. Status of the global electroweak fit with Gfitter in the light of new precision measurements. *PoS*, ICHEP2022:897, 11 2022.

[22] J. de Blas, M. Pierini, L. Reina, and L. Silvestrini. Impact of the Recent Measurements of the Top-Quark and W-Boson Masses on Electroweak Precision Fits. *Phys. Rev. Lett.*, 129(27):271801, 2022.

[23] Armen Tumasyan et al. Search for new physics in the lepton plus missing transverse momentum final state in proton-proton collisions at $\sqrt{s} = 13$ TeV. *JHEP*, 07:067, 2022.

[24] Peter W. Higgs. Broken symmetries and the masses of gauge bosons. *Phys. Rev. Lett.*, 13:508–509, Oct 1964.

[25] Georges Aad et al. Observation of a new particle in the search for the Standard Model Higgs boson with the ATLAS detector at the LHC. *Phys. Lett. B*, 716:1–29, 2012.

[26] Serguei Chatrchyan et al. Observation of a New Boson at a Mass of 125 GeV with the CMS Experiment at the LHC. *Phys. Lett. B*, 716:30–61, 2012.

[27] Steven Weinberg. A Model of Leptons. *Phys. Rev. Lett.*, 19:1264–1266, 1967.

[28] S. L. Glashow. Partial Symmetries of Weak Interactions. *Nucl. Phys.*, 22:579–588, 1961.

[29] Jeffrey Goldstone, Abdus Salam, and Steven Weinberg. Broken Symmetries. *Phys. Rev.*, 127:965–970, 1962.

[30] Amitabha Lahiri and Palash B. Pal. *A First Book of Quantum Field Theory*. 2005.

[31] G. Arnison, A. Astbury, B. Aubert, C. Bacci, G. Bauer, A. Bézaguet, R. Böck, T.J.V. Bowcock, M. Calvetti, T. Carroll, P. Catz, P. Cennini, S. Centro, F. Ceradini, S. Cittolin, D. Cline, C. Cochet, J. Colas, M. Corden, D. Dallman, M. DeBeer, M. Della Negra, M. Demoulin, D. Denegri, A. Di Ciaccio, D. DiBitonto, L. Dobrzynski, J.D. Dowell, M. Edwards, K. Eggert, E. Eisenhandler, N. Ellis, P. Erhard, H. Faissner, G. Fontaine, R. Frey, R. Frühwirth, J. Garvey, S. Geer, C. Ghesquière, P. Ghez, K.L. Giboni, W.R. Gibson, Y. Giraud-Héraud, A. Givernaud, A. Gonidec, G. Grayer, P. Gutierrez, T. Hansl-Kozanecka, W.J. Haynes, L.O. Hertzberger, C. Hodges, D. Hoffmann, H. Hoffmann, D.J. Holthuizen, R.J. Homer, A. Honma, W. Jank, G. Jorat, P.I.P. Kalmus, V. Karimäki, R. Keeler, I. Kenyon, A. Kernan, R. Kinnunen, H. Kowalski, W. Kozanecki, D. Kryn, F. Lacava, J.-P. Laugier, J.-P. Lees, H. Lehmann, K. Leuchs, A. Lévêque, E. Linglin, E. Locci, M. Loret, J.-J. Malosse, T. Markiewicz, G. Maurin, T. McMahon, J.-P. Mendiburu, M.-N. Minard, M. Moricca, H. Muirhead, F. Muller, A.K. Nandi, L. Naumann, A. Norton, A. Orkin-Lecourtois, L. Paoluzi, G. Petrucci, G.Piano Mortari, M. Pimiä, A. Placci, E. Radermacher, J. Ransdell, H. Reithler, J.-P. Revol, J. Rich, M. Rijssenbeek, C. Roberts, J. Rohlf, P. Rossi, C. Rubbia, B. Sadoulet, G. Sajot, G. Salvi, J. Salvini, J. Sass, A. Saudraix, A. Savoy-Navarro, D. Schinzel, W. Scott, T.P. Shah, M. Spiro, J. Strauss, K. Sumorok, F. Szoncso, D. Smith, C. Tao, G. Thompson, J. Timmer, E. Tscheslog, J. Tuominiemi, S. Van der Meer, J.-P. Vialle, J. Vrana, V. Vuillemin, H.D. Wahl, P. Watkins, J. Wilson, Y.G. Xie, M. Yvert,

and E. Zurfluh. Experimental observation of isolated large transverse energy electrons with associated missing energy at s=540 gev. *Physics Letters B*, 122(1):103–116, 1983.

[32] M. Banner, R. Battiston, Ph. Bloch, F. Bonaudi, K. Borer, M. Borghini, J.-C. Chollet, A.G. Clark, C. Conta, P. Darriulat, L. Di Lella, J. Dines-Hansen, P.-A. Dorsaz, L. Fayard, M. Fraternali, D. Froidevaux, J.-M. Gaillard, O. Gildemeister, V.G. Goggi, H. Grote, B. Hahn, H. Hänni, J.R. Hansen, P. Hansen, T. Himel, V. Hungerbühler, P. Jenni, O. Kofoed-Hansen, E. Lançon, M. Livan, S. Loucatos, B. Madsen, P. Mani, B. Mansoulie, G.C. Mantovani, L. Mapelli, B. Merkel, M. Mermikides, R. Møllerud, B. Nilsson, C. Onions, G. Parrour, F. Pastore, H. Plothow-Besch, M. Polverel, J.-P. Repellin, A. Rothenberg, A. Roussarie, G. Sauvage, J. Schacher, J.L. Siegrist, H.M. Steiner, G. Stimpfl, F. Stocker, J. Teiger, V. Vercesi, A. Weidberg, H. Zaccone, and W. Zeller. Observation of single isolated electrons of high transverse momentum in events with missing transverse energy at the cern pp collider. *Physics Letters B*, 122(5):476–485, 1983.

[33] Aleksandra Dimitrievska. Measurement of the W boson mass and the calibration of the muon momentum with the ATLAS detector. Merenje mase W bozona i kalibracija impulsa miona na detektoru ATLAS, 2017. Presented 20 Nov 2017.

[34] Timothy Cohen, Stephanie Majewski, Bryan Ostdiek, and Peter Zheng. On the ATLAS Top Mass Measurements and the Potential for Stealth Stop Contamination. *JHEP*, 06:019, 2020.

[35] Till Eifert and Benjamin Nachman. Sneaky light stop. *Phys. Lett. B*, 743:218–223, 2015.

[36] Roberto Franceschini. Wish-list for Run II top quark measurements (for BSM). In *3rd Large Hadron Collider Physics Conference*, pages 420–425, 2015.

[37] Xiao-Gang He, Girish C. Joshi, H. Lew, and R. R. Volkas. Simplest Z-prime model. *Phys. Rev. D*, 44:2118–2132, 1991.

[38] Gordan Krnjaic, Gustavo Marques-Tavares, Diego Redigolo, and Kohsaku Tobioka. Probing Muonphilic Force Carriers and Dark Matter at Kaon Factories. *Phys. Rev. Lett.*, 124(4):041802, 2020.

[39] Majid Ekhterachian, Anson Hook, Soubhik Kumar, and Yuhsin Tsai. Bounds on gauge bosons coupled to nonconserved currents. *Phys. Rev. D*, 104(3):035034, 2021.

[40] Jeffrey M. Berryman, André De Gouvêa, Kevin J. Kelly, and Yue Zhang. Lepton-Number-Charged Scalars and Neutrino Beamstrahlung. *Phys. Rev. D*, 97(7):075030, 2018.

[41] P. S. Bhupal Dev, Bhaskar Dutta, Tathagata Ghosh, Tao Han, Han Qin, and Yongchao Zhang. Leptonic scalars and collider signatures in a UV-complete model. *JHEP*, 03:068, 2022.

[42] André de Gouvêa and Andrew Kobach. Global Constraints on a Heavy Neutrino. *Phys. Rev. D*, 93(3):033005, 2016.

[43] Bridget Bertoni, Seyda Ipek, David McKeen, and Ann E. Nelson. Constraints and consequences of reducing small scale structure via large dark matter-neutrino interactions. *JHEP*, 04:170, 2015.

[44] Jeff A. Dror, Robert Lasenby, and Maxim Pospelov. New constraints on light vectors coupled to anomalous currents. *Phys. Rev. Lett.*, 119(14):141803, 2017.

[45] Luca Di Luzio, Marco Nardecchia, and Claudio Toni. Light vectors coupled to anomalous currents with harmless Wess-Zumino terms. *Phys. Rev. D*, 105(11):115042, 2022.

[46] Christopher D. Carone and Hitoshi Murayama. Realistic models with a light U(1) gauge boson coupled to baryon number. *Phys. Rev. D*, 52:484–493, 1995.

[47] Pavel Fileviez Perez and Mark B. Wise. Baryon and lepton number as local gauge symmetries. *Phys. Rev. D*, 82:011901, 2010. [Erratum: Phys.Rev.D 82, 079901 (2010)].

[48] Philip Ilten, Yotam Soreq, Mike Williams, and Wei Xue. Serendipity in dark photon searches. *JHEP*, 06:004, 2018.

[49] Jens Boos, Christopher D. Carone, Noah L. Donald, and Mikkie R. Musser. Asymptotically safe dark matter with gauged baryon number. *Phys. Rev. D*, 107(3):035018, 2023.

[50] J. Wess and B. Zumino. A Lagrangian Model Invariant Under Supergauge Transformations. *Phys. Lett. B*, 49:52, 1974.

[51] J. Wess and B. Zumino. Supergauge Invariant Extension of Quantum Electrodynamics. *Nucl. Phys. B*, 78:1, 1974.

[52] J. Wess and B. Zumino. Supergauge Transformations in Four-Dimensions. *Nucl. Phys. B*, 70:39–50, 1974.

[53] D. V. Volkov and V. P. Akulov. Is the Neutrino a Goldstone Particle? *Phys. Lett. B*, 46:109–110, 1973.

[54] Yu. A. Golfand and E. P. Likhtman. Extension of the Algebra of Poincare Group Generators and Violation of p Invariance. *JETP Lett.*, 13:323–326, 1971.

[55] Stephen P. Martin. A Supersymmetry primer. *Adv. Ser. Direct. High Energy Phys.*, 18:1–98, 1998.

[56] Csaba Csaki. The Minimal supersymmetric standard model (MSSM). *Mod. Phys. Lett. A*, 11:599, 1996.

[57] Linda M. Carpenter, Humberto B. Gilmer, and Junichiro Kawamura. New Bounds on Light Sneutrino Masses: Rare SUSY Signals. *Phys. Rev. D*, 103(9):095014, 2021.

[58] Kaustubh Agashe, Sagar Airen, Roberto Franceschini, Doojin Kim, Ashutosh V. Kotwal, Lorenzo Ricci, and Deepak Sathyan. A new purpose for the W-boson mass measurement: searching for New Physics in lepton+MET. 10 2023.

[59] J. Alwall, R. Frederix, S. Frixione, V. Hirschi, F. Maltoni, O. Mattelaer, H. S. Shao, T. Stelzer, P. Torrielli, and M. Zaro. The automated computation of tree-level and next-to-leading order differential cross sections, and their matching to parton shower simulations. *JHEP*, 07:079, 2014.

[60] Christian Bierlich et al. A comprehensive guide to the physics and usage of PYTHIA 8.3. 3 2022.

[61] J. de Favereau, C. Delaere, P. Demin, A. Giammanco, V. Lemaître, A. Mertens, and M. Selvaggi. DELPHES 3, A modular framework for fast simulation of a generic collider experiment. *JHEP*, 02:057, 2014.

[62] Andy Buckley, James Ferrando, Stephen Lloyd, Karl Nordström, Ben Page, Martin Rüfenacht, Marek Schönherr, and Graeme Watt. LHAPDF6: parton density access in the LHC precision era. *The European Physical Journal C*, 75(3), mar 2015.

[63] Richard D. Ball, Valerio Bertone, Stefano Carrazza, Luigi Del Debbio, Stefano Forte, Alberto Guffanti, Nathan P. Hartland, and Juan Rojo. Parton distributions with QED corrections. *Nuclear Physics B*, 877(2):290–320, dec 2013.

[64] Joshua Isaacson, Yao Fu, and C. P. Yuan. ResBos2 and the CDF W Mass Measurement. 5 2022.

[65] Elie Hammou, Zahari Kassabov, Maeve Madigan, Michelangelo L. Mangano, Luca Mantani, James Moore, Manuel Morales Alvarado, and Maria Ubiali. Hide and seek: how PDFs can conceal New Physics. 7 2023.

[66] Triparno Bandyopadhyay, Ankita Budhraja, Samadrita Mukherjee, and Tuhin S. Roy. A twisted tale of the transverse-mass tail. 12 2022.

[67] S. R. Mishra et al. Neutrino Tridents and W Z Interference. *Phys. Rev. Lett.*, 66:3117–3120, 1991.

[68] Brian Batell, Tao Han, David McKeen, and Barmak Shams Es Haghi. Thermal Dark Matter Through the Dirac Neutrino Portal. *Phys. Rev. D*, 97(7):075016, 2018.

[69] Kaustubh Agashe, Sagar Airen, Roberto Franceschini, Doojin Kim, Ashutosh V. Kotwal, Lorenzo Ricci, and Deepak Sathyan. in preparation.

[70] P. S. Bhupal Dev, Doojin Kim, Deepak Sathyan, Kuver Sinha, and Yongchao Zhang. New Laboratory Constraints on Neutrinophilic Mediators. 7 2024.

[71] Georges Aad et al. Search for new phenomena in events with an energetic jet and missing transverse momentum in pp collisions at $\sqrt{s}$ =13 TeV with the ATLAS detector. *Phys. Rev. D*, 103(11):112006, 2021.

[72] C. Degrande, C. Duhr, B. Fuks, D. Grellscheid, O. Mattelaer, and T. Reiter. UFO - The Universal FEYNRULES Output. *Computer Physics Communications*, 183:1201–1214, June 2012.

[73] Andreas Albert, Mihailo Backovic, Antonio Boveia, Oliver Buchmueller, Giorgio Busoni, Albert De Roeck, Caterina Doglioni, Tristan DuPree, Malcolm Fairbairn, Marie-Helene Genest, Stefania Gori, Giuliano Gustavino, Kristian Hahn, Ulrich Haisch, Philip C. Harris, Dan Hayden, Valerio Ippolito, Isabelle John, Felix Kahlhoefer, Suchita Kulkarni, Greg Landsberg, Steven Lowette, Kentarou Mawatari, Antonio Riotto, William Shepherd, Tim M. P. Tait, Emma Tolley, Patrick Tunney, Bryan Zaldivar, and Markus Zinser. Recommendations of the LHC Dark Matter Working Group: Comparing LHC searches for heavy mediators of dark matter production in visible and invisible decay channels. *arXiv e-prints*, page arXiv:1703.05703, March 2017.

[74] A. Boveia, O. Buchmueller, G. Busoni, F. D'Eramo, A. De Roeck, A. De Simone, C. Doglioni, M. J. Dolan, M.-H. Genest, K. Hahn, U. Haisch, P. C. Harris, J. Heisig, V. Ippolito, F. Kahlhoefer, V. V. Khoze, S. Kulkarni, G. Landsberg, S. Lowette, S. Malik, M. Mangano, C. McCabe, S. Mrenna, P. Pani, T. du Pree, A. Riotto, D. Salek, K. Schmidt-Hoberg, W. Shepherd, T. M. P. Tait, L.-T. Wang, S. Worm, and K. Zurek. Recommendations on presenting LHC searches for missing transverse energy signals using simplified s-channel models of dark matter. March 2016.

[75] A. Heister et al. Search for scalar leptons in e+ e- collisions at center-of-mass energies up to 209-GeV. *Phys. Lett. B*, 526:206–220, 2002.

[76] A. Heister et al. Absolute mass lower limit for the lightest neutralino of the MSSM from e+ e- data at s**(1/2) up to 209-GeV. *Phys. Lett. B*, 583:247–263, 2004.

[77] J. Abdallah et al. Searches for supersymmetric particles in e+ e- collisions up to 208-GeV and interpretation of the results within the MSSM. *Eur. Phys. J. C*, 31:421–479, 2003.

[78] P. Achard et al. Search for scalar leptons and scalar quarks at LEP. *Phys. Lett. B*, 580:37–49, 2004.

[79] G. Abbiendi et al. Search for anomalous production of dilepton events with missing transverse momentum in e+ e- collisions at s**(1/2) = 183-Gev to 209-GeV. *Eur. Phys. J. C*, 32:453–473, 2004.

[80] Combined search for electroweak production of winos, binos, higgsinos, and sleptons in proton-proton collisions at $sqrts =$ 13 TeV. Technical report, CERN, Geneva, 2023.

[81] David Curtin, Prerit Jaiswal, and Patrick Meade. Charginos Hiding In Plain Sight. *Phys. Rev. D*, 87(3):031701, 2013.

[82] David Curtin, Prerit Jaiswal, Patrick Meade, and Pin-Ju Tien. Casting Light on BSM Physics with SM Standard Candles. *JHEP*, 08:068, 2013.

[83] Georges Aad et al. Search for electroweak production of charginos and sleptons decaying into final states with two leptons and missing transverse momentum in $\sqrt{s} = 13$ TeV pp collisions using the ATLAS detector. *Eur. Phys. J. C*, 80(2):123, 2020.

[84] Nilendra G. Deshpande and Ernest Ma. Pattern of Symmetry Breaking with Two Higgs Doublets. *Phys. Rev. D*, 18:2574, 1978.

[85] Riccardo Barbieri, Lawrence J. Hall, and Vyacheslav S. Rychkov. Improved naturalness with a heavy Higgs: An Alternative road to LHC physics. *Phys. Rev. D*, 74:015007, 2006.

[86] Qing-Hong Cao, Ernest Ma, and G. Rajasekaran. Observing the Dark Scalar Doublet and its Impact on the Standard-Model Higgs Boson at Colliders. *Phys. Rev. D*, 76:095011, 2007.

[87] Jan Kalinowski, Tania Robens, Dorota Sokolowska, and Aleksander Filip Zarnecki. IDM Benchmarks for the LHC and Future Colliders. *Symmetry*, 13(6):991, 2021.